Mon. Not. R. Astron. Soc. **350,** 407–426 (2004) doi:10.1111/j.1365-2966.2004.07446.x

A new synthetic model for asymptotic giant branch stars

Robert G. Izzard,[1⋆] Christopher A. Tout,[1] Amanda I. Karakas[2,3] and Onno R. Pols[4]

[1] *Institute of Astronomy, Madingley Road, Cambridge CB3 0HA*
[2] *School of Mathematical Sciences, Monash University, Wellington Road, Clayton, Victoria 3800, Australia*
[3] *Institute for Computational Astrophysics, Department of Astronomy & Physics, Saint Mary's University, Halifax, NS B3H 3C3, Canada*
[4] *Astronomical Institute Utrecht, Postbus 80000, 3508 TA Utrecht, the Netherlands*

Accepted 2003 November 21. Received 2003 November 21; in original form 2003 January 23

ABSTRACT

We present a synthetic model for thermally pulsing asymptotic giant branch (TPAGB) evolution constructed by fitting expressions to full evolutionary models in the metallicity range $0.0001 \leqslant Z \leqslant 0.02$. Our model includes parametrizations of third dredge-up and hot-bottom burning with mass and metallicity. The Large Magellanic Cloud and Small Magellanic Cloud carbon star luminosity functions are used to calibrate third dredge-up. We calculate yields appropriate for galactic chemical evolution models for ^{1}H, ^{4}He, ^{12}C, ^{13}C, ^{14}N, ^{15}N, ^{16}O and ^{17}O. The initial–final mass relation is examined for our stars and found to fit to within 0.1 $M_{\odot}$ of the observations. We also reproduce well the white dwarf mass function for masses above about 0.58 $M_{\odot}$. The new model is to be implemented in a rapid binary star evolution code.

Key words: stars: AGB and post-AGB – stars: carbon – ISM: abundances.

1 INTRODUCTION

Full stellar evolution models of thermally pulsing asymptotic giant branch (TPAGB) stars are difficult and extremely time-consuming to make, and often suffer numerical failure. For this reason, synthetic models based on full stellar evolution models but with the complicated physics replaced by simple expressions are a useful approximation. Such models are well suited to exploring regions of large, multidimensional parameter spaces which would take years to explore with full stellar evolution models. Here we build on the models of Groenewegen & de Jong (1993) and Wagenhuber & Groenewegen (1998) with accurate new parametrizations of third dredge-up and hot-bottom burning (HBB), as well as new fits to stellar structure from our full stellar evolution models. Stellar evolution up to the TPAGB is handled by coupling the new code with the rapid evolution code of Hurley, Pols & Tout (2000) and Hurley, Tout & Pols (2002, H02) which is designed for single, binary and star cluster evolution. The eventual aim of this work is to implement TPAGB evolution and especially nucleosynthesis in the binary star model and, while this is yet some way off, we have made significant progress in constructing a capable single star model. The calculation of binary star yields will result.

Table 1, mostly taken from the review of Henry (2004), summarizes attempts at calculating AGB yields to date. It does not include important works on AGB evolution that do not specifically involve yield calculation, such as the series of works by Boothroyd & Sackmann (e.g. Boothroyd & Sackmann 1988) who investigate Li, Be, B and ^{12}C/^{13}C ratios in particular, Straniero et al. (1997) who tackle the carbon star formation problem in low-mass ($1 \leqslant M/M_{\odot} \leqslant 3$) solar-metallicity stars, Lattanzio and collaborators' contribution to HBB (Lattanzio et al. 1997), carbon star formation (Lattanzio 1989) and degenerate pulses (Frost, Lattanzio & Wood 1998), Mowlavi and collaborators' works on ^{26}Al (Mowlavi & Meynet 2000), fluorine (Mowlavi, Jorissen & Arnould 1998) and sodium (Mowlavi 1999), and models by Herwig (2000) detailing convective overshooting and its consequences. There are also countless papers dealing specifically with the s-process in TPAGB stars (e.g. Busso et al. 2001).

Synthetic models have been constructed in the past (e.g. Renzini & Voli 1981; Iben & Renzini 1983) and are still very much in use (Mouhcine & Lançon 2003). Hybrid models which combine aspects of synthetic and full evolution have also been constructed (Marigo, Bressan & Chiosi 1998; Marigo 1999, 2001). While we lean heavily on the work of Groenewegen & de Jong (1993) and Wagenhuber & Groenewegen (1998), our new model has some marked differences in its treatment of dredge-up and HBB. Most previous models assume a constant dredge-up parameter and minimum core mass for dredge-up. We include expressions fitted to our full stellar evolution models (Karakas, Lattanzio & Pols 2002) for these and the stellar structure (luminosity, radius, core mass, etc.). HBB is included in a similar way to Groenewegen & de Jong (1993) but with calibration of the free parameters to our full evolution models.

While the use of a purely synthetic code is inferior in accuracy or detail to full stellar modelling [or the envelope burning technique of Marigo 1999a (M99)], it is the only way to explore a large parameter space such as a full study of binary stars. The single star space could conceivably consist of the mass M, metallicity Z and a few free parameters such as the minimum mass for dredge-up, dredge-up efficiency and perhaps the mass-loss rate. For binaries the problem

⋆E-mail: rgi@ast.cam.ac.uk

Table 1. Summary of existing TPAGB models. IT = Iben & Truran (1978); RV = Renzini & Voli (1981); HG = van den Hoek & Groenewegen (1997); FC = Forestini & Charbonnel (1997); M01 = Marigo (2001); C01 = Chieffi et al. (2001); K02 = Karakas et al. (2002); D03 = Dray et al. (2003). 'Syn' indicates a synthetic TPAGB code; 'SynEnv' denotes a synthetic TPAGB code with envelope integration; 'Full' are full stellar evolution models covering the TPAGB. The HBB column contains 'n' = no, 'a' = analytic, and 'net' nuclear network ('extrap' is an extrapolation from full network calculations).

Authors	Mass range ($M_\odot$)	Z range	HBB	Isotopes	Model type	Extras
IT	1–8	0.02	n	^{12,13}C, ^{14}N,^{22}Ne	Syn	
RV	1–8	0.004–0.02	a	^{12,13}C, ^{14}N,^{16}O	Syn	
HG	0.8–8	0.001–0.04	a	^{12,13}C, ^{14}N,^{16}O	Syn	
FC	3–7	0.005-0.02	net/extrap	many	Syn/Full	
M01	0.8–6	0.004–0.019	net	^{12,13}C, ^{14,15}N,^{16,17,18}O	SynEnv	
C01	4–8	0	net	many	Full	
K02/D03	1–6(.5)	$0.004 - 0.02$	net	many	Full	
Our model	1–8	10^{-4}–0.03	a	^{12,13}C, ^{14,15}N,^{16,17}O,^{22}Ne so far	Syn	Binaries

Table 2. List of variables.

Symbol	Meaning
Z	ZAMS metallicity ($Z_\odot = 0.02$)
M_i	ZAMS mass
M	Instantaneous mass
M_c	Instantaneous core mass
$M_{\mathrm{c,bagb}}$	Core mass at the base of the (E)AGB
$M_{\mathrm{c,1TP}}$	Core mass at the start of the TPAGB
M_{1TP}	Mass at the start of the TPAGB
M_env	Envelope mass, calculated from $M - M_\mathrm{c}$
$M_{\mathrm{env,1TP}}$	Envelope mass at the start of the TPAGB
X_i	Mass fraction of isotope i
$\dot{M}$	Stellar mass-loss rate
ζ	$\log_{10}(Z/0.02)$

is worse, there are the two masses, separation and eccentricity, and in addition free parameters associated with uncertain details of common-envelope evolution, mass transfer and accretion and enhanced wind loss owing to the companion. A parameter space takes a time $\delta t \times n^N$ to explore, where δt is the average model time, n is the number of grid-points per free parameter and N is the number of free parameters, so a fast model is desired. Our model has an average execution time (including features not described here, such as a companion star and associated mass transfer, NeNa and MgAl cycles, supernovae and novae) of 0.05 s on a 2.1-GHz AMD Athlon CPU[1] (0.64 s on a Pentium Pro 200-MHz CPU[2]), so for a 10^6-point grid we have a total execution time of nearly 14 h. An increase of δt to 1 min (which would be an extremely fast full stellar evolution model) increases the total execution time to just less than 2 years.

The drawback of a fast code is a loss of accuracy and, while we try to fit to our full evolution models as well as we can, it is impossible to fit perfectly. We have to interpolate and sometimes extrapolate into regions of parameter space where we cannot be sure that we get the correct answer. Since we aim to investigate binary stars with this code, we put up with these limitations and keep in mind that detailed models of binary stars may differ. There are some things that a synthetic model avoids, such as numerical breakdown which can occur with a full evolution model. The synthetic model is no worse than our detailed model for star-to-star analyses.

Table 2 lists some common variables used in this paper. Section 2 describes our full stellar evolution models. Section 3 contains the (gory) details of our synthetic model. Detailed calibration and analysis of the variation in the free parameters introduced in the HBB model are made in Section 4. Calibration of third dredge-up using carbon star luminosity functions is described in Section 5.1. The initial–final mass relation and white dwarf mass functions derived from the model are compared with observations in Sections 5.4 and 5.5. Yields from single stars are calculated in Section 6 with comparison to our full stellar evolution model yields and the yields of van den Hoek & Groenewegen (1997) and Marigo (2001). The appendix (in the online version of the article only[3]) contains the coefficients for the fitting formulae, yield tables and synthetic-detailed model composition comparisons.

2 FULL EVOLUTIONARY MODELS

Our full stellar evolution models used are those described in Karakas et al. (2002) (hereafter K02). They were constructed with the Monash version of the Mt Stromlo Stellar Evolution Code (Wood & Zarro 1981; Frost 1997) updated to use the OPAL opacity tables of Iglesias & Rogers (1996). The thermally pulsing phase of the AGB is covered by the models until mass loss makes convergence impossible. Mass loss is parametrized on the red giant branch using the Kudritzki & Reimers (1978) formula with $\eta = 0.4$ and on the AGB using the prescription of (Vassiliadis & Wood 1993, VW93). The mixing length parameter α is set to 1.75 and convective overshooting is not included in the models.

We have high-resolution evolution (taken every 100 models from the stellar structure code) and nucleosynthesis model data for $Z = 0.02$, $M_\mathrm{i} = 3, 4, 5, 6, 6.5\ \mathrm{M}_\odot$, $Z = 0.008$, $M_\mathrm{i} = 4, 5, 6\ \mathrm{M}_\odot$, $Z = 0.004$, $M_\mathrm{i} = 4, 5, 6\ \mathrm{M}_\odot$ and $Z = 0.0001$, $M_\mathrm{i} = 1.25, 2, 2.25\ \mathrm{M}_\odot$, and lower resolution data (every 1000 stellar structure models) for $Z = 0.02$, $M_\mathrm{i} = 1, 1.25, 1.9, 2.5, 3.5\ \mathrm{M}_\odot$, $Z = 0.008$, $M_\mathrm{i} = 1, 1.9, 2.5, 3, 3.5\ \mathrm{M}_\odot$, $Z = 0.004$, $M_\mathrm{i} = 1, 2, 2.5, 3, 3.5\ \mathrm{M}_\odot$ and $Z = 0.0001$, $M_\mathrm{i} = 1.75\ \mathrm{M}_\odot$, where M_i is the initial (zero-age main-sequence, ZAMS) mass of the star. There are typically a few thousand evolutionary models per interpulse period.

3 OUR SYNTHETIC MODEL

Stellar evolution from the ZAMS up to the thermally pulsing AGB is already dealt with in the rapid evolution code (Hurley, Pols & Tout 2000). The main sequence, giant branch evolution and early AGB (EAGB) abundance changes can be represented by simple formulae dealing with first and second dredge-up. All abundances are mass

[1] Manufacturer: AMD, One AMD Place, PO Box 3453, Sunnyvale, CA 95070, USA

[2] Manufacturer: Intel, 2000 Mission College Blvd., Santa Clara, CA 95052, USA

[3] http://www.blackwellpublishing.com/products/journals/suppmat/mnr/mnr7446/mnr7446sm.htm

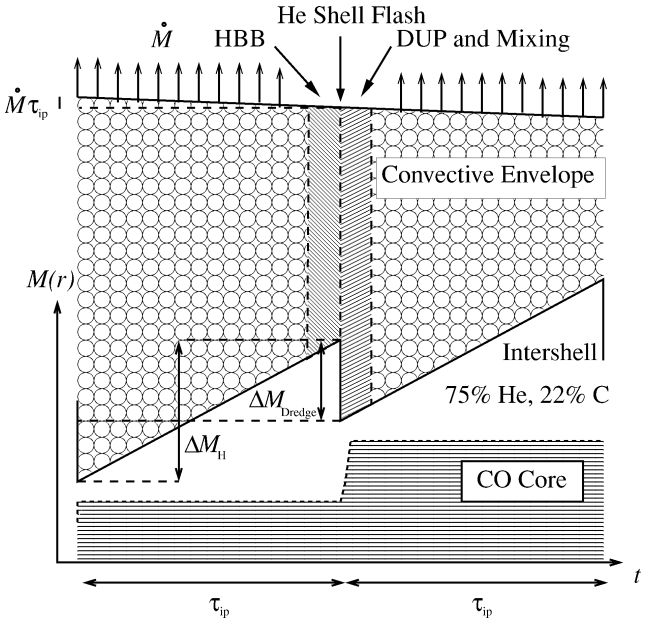

Figure 1. Time evolution of our synthetic AGB model ($\lambda > 0$, not to scale). During the interpulse period τ_{ip} the hydrogen-free core M_c (Intershell + CO Core) grows by ΔM_H and the envelope loses mass $\dot{M}\tau_{ip}$. At the end of the time-step (usually the end of the interpulse period) we burn the envelope using the HBB algorithm and then a He-shell flash occurs causing $\Delta M_{dredge} = \lambda \Delta M_H$ of material from the intershell region to mix with the convective envelope. The new interpulse period τ'_{ip} is calculated and the evolution continued. The CO core is shown here but we consider it to have the same mass as the hydrogen-free core.

fractions. Coefficients for fits are in Appendix A[4] unless otherwise stated. The fits are made using a Levenberg–Marquardt gradient descent iterative χ^2-minimization code (Press et al. 1992).

The state of the star at the beginning of the TPAGB is known from the fits given in Sections 3.2 and 3.3. The star is evolved forward in time pulse by pulse (see Fig. 1). Between pulses the star loses mass at a rate $\dot{M}$ from the envelope in a wind. The core grows owing to hydrogen burning and the envelope material may experience HBB. At every time-step (usually coincident with a thermal pulse) the HBB algorithm is activated and, if the time since the previous pulse exceeds the interpulse period, is immediately followed by third dredge-up. The change in core mass due to nuclear burning and dredge-up combined with the effect of wind loss (see Section 3.6) determines the time evolution of the star.

The rapid stellar evolution code defines a time-step δt such that certain variables (e.g. radius or angular momentum) may not change by a large amount during that time-step. We add an additional constraint that the time-step must be at most the interpulse period. Because we expect the time-step to be the same as the interpulse period most of the time (especially for detached binaries), luminosity variations owing to the pulse cycle are averaged out, although luminosity changes owing to an increase in core mass are followed if the time-step is small enough.

3.1 From the ZAMS to EAGB

Stellar evolution on the main sequence does not affect the surface abundances, except in some rare cases not considered here (e.g. when the lifetime of the star is long enough that diffusion becomes an important transport mechanism). Only during hydrogen shell burning, when the star is a red giant, does the convective envelope reach down into burned material and mix the products of nuclear processing. This mixing event changes the surface abundances and is known as the first dredge-up. A similar process takes place during the early AGB when second dredge-up follows the transition to helium shell burning.

[4] http://www.blackwellpublishing.com/products/journals/suppmat/mnr/mnr7446/mnr7446sm.htm

Table 3. ZAMS abundances (mass fractions) used in both the full stellar evolution models and the synthetic models for $Z = 0.02, 0.008$ and 0.004 (first row of numbers for each species) and the equivalent solar-scaled abundance (second row of numbers).

Z	0.02	0.008	0.004
^{1}H	0.687 20	0.736 89	0.748 40
^{4}He	0.292 80	0.255 10	0.247 60
^{12}C	$2.925\,93 \times 10^{-3}$	$9.695\,93 \times 10^{-4}$	$4.822\,97 \times 10^{-4}$
		$1.170\,37 \times 10^{-3}$	$5.851\,86 \times 10^{-4}$
^{13}C	$4.108\,00 \times 10^{-5}$	$2.882\,81 \times 10^{-5}$	$1.499\,27 \times 10^{-5}$
		1.6432×10^{-5}	8.216×10^{-6}
^{14}N	$8.978\,64 \times 10^{-4}$	$1.424\,08 \times 10^{-4}$	$5.108\,03 \times 10^{-5}$
		$3.591\,46 \times 10^{-4}$	$1.795\,73 \times 10^{-4}$
^{15}N	$4.140\,00 \times 10^{-6}$	$2.905\,00 \times 10^{-6}$	$1.510\,90 \times 10^{-6}$
		1.656×10^{-6}	8.28×10^{-7}
^{16}O	$8.150\,85 \times 10^{-3}$	$2.639\,54 \times 10^{-3}$	$1.283\,08 \times 10^{-3}$
		$3.260\,34 \times 10^{-3}$	$1.630\,17 \times 10^{-3}$
^{17}O	$3.876\,00 \times 10^{-6}$	$2.720\,00 \times 10^{-6}$	$1.414\,59 \times 10^{-6}$
		1.5504×10^{-6}	7.752×10^{-7}
^{22}Ne	$1.452\,00 \times 10^{-4}$	$1.018\,94 \times 10^{-4}$	$5.299\,27 \times 10^{-5}$
		5.8088×10^{-5}	2.904×10^{-5}

3.1.1 Initial abundances

ZAMS abundances are identical to our full stellar evolutionary models [taken from Anders & Grevesse (1989) for $Z = 0.02$ and Russell & Dopita (1992) for $Z = 0.008$ and 0.004] shown in Table 3. Quadratic fits are used for $0.02 \leqslant Z \leqslant 0.004$ such that each isotope i has an abundance given by

$$X_i = \left(a_{i,1} + b_{i,1}Z + c_{i,1}Z^2\right), \tag{1}$$

with the coefficients given in Appendix A. The fits are exact for the metallicities of our full stellar evolution models. The $Z = 0.0001$ models use scaled solar abundances (Anders & Grevesse 1989) so we do likewise. Table 3 also shows the solar-scaled abundances for $Z = 0.008$ and 0.004 in order to highlight the differences between the two sets.

To some extent the synthetic model is independent of the initial abundances because HBB is dealt with by solution of the appropriate differential equations. Abundance changes at first, second and third dredge-up are independent of modest changes in the initial abundances because, to first order, the stellar structure does not depend on the abundance mix at a given Z.

3.1.2 First dredge-up

Stars that undergo first dredge-up during their first ascent of the giant branch have their abundances modified by

$$\Delta X = \begin{cases} -0.017M + 0.01125Z, & M/\mathrm{M}_\odot < 2; \\ -0.004M + & \\ 0.0074Z(M/\mathrm{M}_\odot - 2), & 2 \leqslant M/\mathrm{M}_\odot < 3.25; \\ 0, & \text{otherwise.} \end{cases} \tag{2}$$

Then $X'_{H1} = X_{H1} - \Delta X$ and $X'_{He4} = X_{He4} + \Delta X$ (i.e. $\Delta X_{He4} = -\Delta X_{H1}$). The CNO abundances are changed by

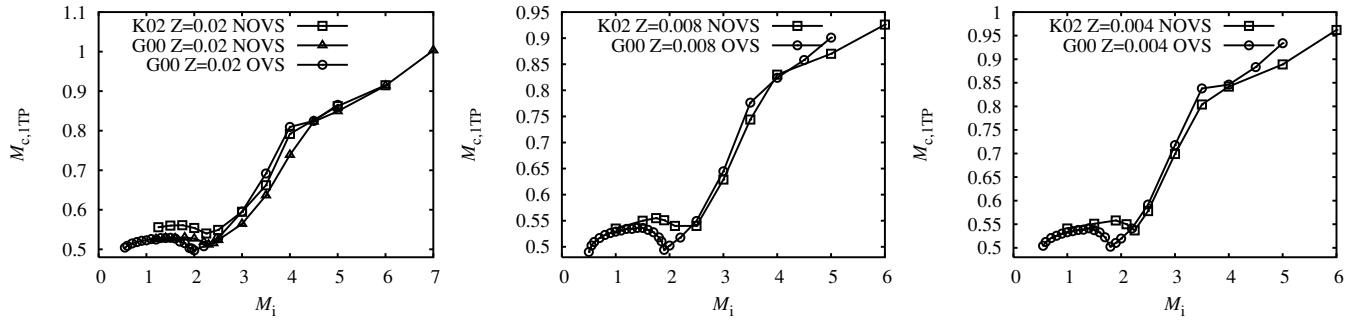

Figure 2. Core mass at the first thermal pulse from our full stellar evolution models (K02) and the Padova group models (G00) for $Z = 0.02$, 0.008 and 0.004. NOVS indicates models without convective overshooting; OVS indicates convective overshooting.

$$g = X_{\rm C12} \times \min(0.36, 0.21 + 0.05M/{\rm M}_\odot) \quad (3)$$

such that

$$X'_{\rm C12} = X_{\rm C12} - g, \quad (4)$$

$$X'_{\rm N14} = X_{\rm N14} + \frac{7}{6}g \quad (5)$$

and

$$X'_{\rm O16} = 0.99X_{\rm O16}. \quad (6)$$

The minority species are fitted to our full stellar evolution models:

$$X'_{\rm C13} = X_{\rm C13} + \left(a_7 + b_7M + c_7M^2 + d_7M^3\right) \times \left(1 + e_7Z + f_7Z^2 - g_7/Z\right), \quad (7)$$

$$X'_{\rm N15} = X_{\rm N15} + \max\Big[-0.5X_{\rm N15}, \left(a_8 + b_8M + c_8M^2 + d_8M^3\right) \times (1 + e_8Z)\Big]\Big/(f_8 + g_8Z), \quad (8)$$

$$X'_{\rm O17} = X_{\rm O17} + \left(a_9 + b_9M + c_9M^2 + d_9M^3\right)(1 + e_9Z) \quad (9)$$

and

$$X'_{\rm Ne22} = X_{\rm Ne22} + \max\left[0, \left(a_{10} + b_{10}M + c_{10}M^2 + d_{10}M^3\right)\left(1 + e_{10}Z + f_{10}Z^2\right)\right]. \quad (10)$$

Our treatment of first dredge-up is similar to that of Renzini & Voli (1981) and (GdJ93 Groenewegen & de Jong 1993 GdJ93) but with the numbers changed to fit our full stellar evolution models better and with an extension to include the minority species. We do not include any extra mixing process on the upper red giant branch.

3.1.3 Second dredge-up

Second dredge-up occurs in sufficiently massive stars [$M_{\rm c,bagb} \geqslant 0.8$ M$_\odot$ where $M_{\rm c,bagb}$ is the core mass of the star at the start of the (E)AGB: see Hurley et al. (2000)] at the end of the EAGB when twin shell burning begins. The Hurley et al. (2000) value for $M_{\rm c,bagb}$ was calculated using overshooting models while our $M_{\rm c,1TP}$ was calculated using non-overshooting models, so there is an inherent inconsistency. However, as shown in Fig. 2, the effect of overshooting on $M_{\rm c,1TP}$ is small. Again following Renzini & Voli (1981) and GdJ93, with alterations to fit our full stellar evolution models better, we define

$$a = \frac{M - M_{\rm c,bagb}}{M - M_{\rm c}^{\rm A}} \quad (11)$$

and

$$b = \frac{M_{\rm c,bagb} - M_{\rm c}^{\rm A}}{M - M_{\rm c}^{\rm A}}, \quad (12)$$

where $M_{\rm c}^{\rm A}$ is the core mass just after second dredge-up, which is assumed to be equal to the core mass at the first thermal pulse (see Section 3.2). Then

$$X'_{\rm H1} = X_{\rm H1} - \Delta X_{\rm H1}, \quad (13)$$

$$X'_{\rm He4} = X_{\rm He4} + \Delta X_{\rm H1}, \quad (14)$$

$$X'_{\rm C12} = aX_{\rm C12}, \quad (15)$$

$$X'_{\rm C13} = aX_{\rm C13}, \quad (16)$$

$$X'_{\rm N14} = aX_{\rm N14} + 14b\left(\frac{X_{\rm C12}}{12} + \frac{X_{\rm C13}}{13} + \frac{X_{\rm N14}}{14} + \frac{X_{\rm N15}}{15} + \frac{X_{\rm O16}}{16} + \frac{X_{\rm O17}}{17}\right), \quad (17)$$

$$X'_{\rm N15} = aX_{\rm N15}, \quad (18)$$

$$X'_{\rm O16} = aX_{\rm O16}, \quad (19)$$

$$X'_{\rm O17} = aX_{\rm O17}, \quad (20)$$

$$X'_{\rm Ne22} = X_{\rm Ne22} + \left(a_{21} + b_{21}M + c_{21}M^2 + d_{21}M^3 + e_{21}M^4\right) \times \left(1 + g_{21}Z + h_{21}Z^2 + i_{21}Z^3\right), \quad (21)$$

where

$$\Delta X_{\rm H1} = a_{22} + b_{22}a + c_{22}Z. \quad (22)$$

Equation (16) is different from GdJ93, who set $X'_{\rm C13} = 0$.

3.2 The start of the TPAGB

On the TPAGB a star consists of a hydrogen-rich convective envelope and a hydrogen-deficient core. The core is defined here as the mass inside which the hydrogen abundance is less than half the surface abundance [$\lesssim$35 per cent by mass, as in Wagenhuber & Groenewegen (1998).[5]] The envelope is assumed to be fully convective.[6]

[5] This definition is not the same as some others in the literature, with the exception of Wagenhuber & Groenewegen (1998), but because the difference in mass coordinate between the He- and H-burning shells is very small, our definition is almost coincidental with any other sensible definition.

[6] This implies that our model is only good for isotopes with nuclear timescales longer than the convective turnover time. We cannot use our model to study e.g. ^{7}Be or ^{7}Li.

At the beginning of the TPAGB we calculate the core mass (Section 3.2.1) as a function of initial TPAGB mass $M_{1\rm TP}$ and metallicity Z. The luminosity, radius and initial interpulse period are then calculated.

3.2.1 Mass and core mass

The fit for the core mass at the first thermal pulse, $M_{\rm c,1TP}$, valid for the range $0.004 \leqslant Z \leqslant 0.02$ and $1 \leqslant M_{1\rm TP}/{\rm M}_\odot \leqslant 6$, is taken from K02:

$$M_{\rm c,1TP}/{\rm M}_\odot = f_{23}\left[-a_{23}(M_{1\rm TP}/{\rm M}_\odot - b_{23})^2 + c_{23}\right] + (1 - f_{23})(d_{23}M_{1\rm TP}/{\rm M}_\odot + e_{23}), \quad (23)$$

where

$$f_{23} = \left[1 + {\rm e}^{(M_{1\rm TP}/{\rm M}_\odot - g_{23})/h_{23}}\right]. \quad (24)$$

The coefficients a_{23} to h_{23} are metallicity-dependent and are interpolated from the tables in K02. Upon extrapolation this function is well-behaved for $0.02 < Z \leqslant 0.03$. We have initial core masses for $Z = 0.0001$ and $M_{\rm i} \leqslant 2.25$ which lead to a fit similar to that for $Z = 0.004$ with a slightly modified f_{23} to take into account the higher core mass at very low metallicity. We assume there is little mass loss prior to the TPAGB, which is true for all but the lowest mass stars which experience significant mass loss on the giant branch, so $M_{1\rm TP} \approx M_{\rm i}$. K02 find little change in $M_{\rm c,1TP}$ whether mass loss is included or not because the $M_{\rm c,1TP}(M_{\rm i})$ curve flattens off at low mass so giant branch mass loss is not important.

Our initial core masses are compared with the models of the Padova group (Girardi et al. 2000, hereafter G00, as used by Marigo 2001) in Fig. 2. The G00 convective overshooting models (which are evolved without mass loss) all have a dip in $M_{\rm c,1TP}$ at around 2 $\rm M_\odot$ which is not so pronounced in any of the non-overshooting models. The G00 models have a lower $M_{\rm c,1TP}$ by up to a few hundredths of a solar mass for $M_{1\rm TP} < 3$ $\rm M_\odot$.

3.3 Evolution on the TPAGB as a function of M, $M_{\rm c}$ and Z

In order to evolve the star forward in time, the interpulse period, luminosity and radius are required as functions of M, $M_{\rm c}$ and Z. We avoid a direct fit to the time, t, so we can vary the mass-loss rate and use the code for binary stars. For some of the fits we use $M_{\rm c,nodup}$, the core mass as it would be in the absence of third dredge-up, defined by

$$M_{\rm c,nodup}(t) = M_{\rm c,1TP} + \int_{t_{1\rm TP}}^{t} \max\left(0, \frac{{\rm d}M_c}{{\rm d}t}\right) {\rm d}t, \quad (25)$$

where $t_{1\rm TP}$ is the time of the first thermal pulse. The use of $M_{\rm c,nodup}$ allows us to account for effects due to an increase in degeneracy in the core during core growth so that two stars with the same core mass yet different age have (for example) a different luminosity.

We also define the change in core mass

$$\Delta M_{\rm c} = M_{\rm c} - M_{\rm c,1TP}, \quad (26)$$

and the change in core mass without third dredge-up

$$\Delta M_{\rm c,nodup} = M_{\rm c,nodup} - M_{\rm c,1TP}. \quad (27)$$

Other fits are to $M_{1\rm TP}$, $M_{\rm c,1TP}$ or N, the thermal pulse number.

3.3.1 Interpulse period

The interpulse period $\tau_{\rm ip}$ is based on the formula in Wagenhuber & Groenewegen (1998), but modified to fit our full stellar evolution models and include a dependence on the dredge-up parameter λ (defined in Section 3.4):

$$\log_{10}(\tau_{\rm ip}/{\rm yr}) = a_{28}(M_{\rm c}/{\rm M}_\odot - b_{28}) - 10^{c_{28}} - 10^{d_{28}} + 0.15\lambda^2, \quad (28)$$

where c_{28} and d_{28} are taken directly from Wagenhuber & Groenewegen (1998). The added coefficients a_{28} and b_{28} are interpolated from the table in Appendix A.

3.3.2 Luminosity

For low-mass stars the peak luminosity at each pulse (after the first few thermal pulses) follows a linear core-mass–luminosity relation (CMLR, Paczynski 1970). For intermediate-mass stars ($M_{\rm i} \gtrsim 3.5$ $\rm M_\odot$) this relation fails because of HBB (Blöcker & Schönberner 1991; Marigo et al. 1999b). We fit the peak luminosity as a sum of the core-mass–luminosity and a term due to HBB:

$$L = f_{\rm d}(f_{\rm t}L_{\rm CMLR} + L_{\rm env})\,{\rm L}_\odot. \quad (29)$$

The CMLR is given by a quadratic in $M_{\rm c}$ for high initial core masses; otherwise a linear form is more suitable. If $M_{\rm c,1TP} > 0.58$,

$$L_{\rm CMLR} = 3.7311 \times 10^4 \times \max\left[(M_{\rm c}/{\rm M}_\odot - 0.52629)(2.7812 - M_{\rm c}/{\rm M}_\odot), 1.2(M_{\rm c}/{\rm M}_\odot - 0.48)\right]; \quad (30)$$

otherwise

$$L_{\rm CMLR} = \max\left[4(18160 + 3980Z)(M_{\rm c} - 0.4468) - 4000, 10\right]. \quad (31)$$

We have no fit for $M_{\rm c} < M_{\rm c,1TP}$, so the above expression is used for $M_{\rm c} > 0.4468$; otherwise the expression from H02 is used (stars with such a low core mass can only form in binary systems).

The envelope luminosity is given by

$$L_{\rm env} = 1.50 \times 10^4 M_{\rm env}^2 \left[1 + 0.75\left(1 - \frac{Z}{0.02}\right)\right] \times \max\left[\left(M_{\rm c}/{\rm M}_\odot + \frac{1}{2}\Delta M_{\rm c,nodup}/{\rm M}_\odot - 0.75\right)^2, 0\right], \quad (32)$$

with a turn-on factor for the first few pulses

$$f_{\rm t} = \min\left[\left(\frac{\Delta M_{\rm c,nodup}}{0.04}\right)^{0.2}, 1.0\right]. \quad (33)$$

In our standard model we do not model the short-time-scale changes in luminosity which occur during the thermal pulse cycle, but it is necessary to correct for these to obtain an accurate evolution algorithm. This is done with the factor $f_{\rm d}$ given by

$$f_{\rm d} = 1 - 0.2180\exp[-11.613(M_{\rm c}/{\rm M}_\odot - 0.56189)]. \quad (34)$$

The luminosity is not allowed to fall below the luminosity of a zero-age white dwarf (taken from H02) with the same mass as the core. Fig. 3 shows our luminosity (full stellar evolution and synthetic models) versus core mass.

3.3.3 Radius

The radius R is defined by $L = 4\pi\sigma R^2 T_{\rm eff}^4$, where σ is the Stefan–Boltzmann constant and $T_{\rm eff}$ is the effective temperature of the star.

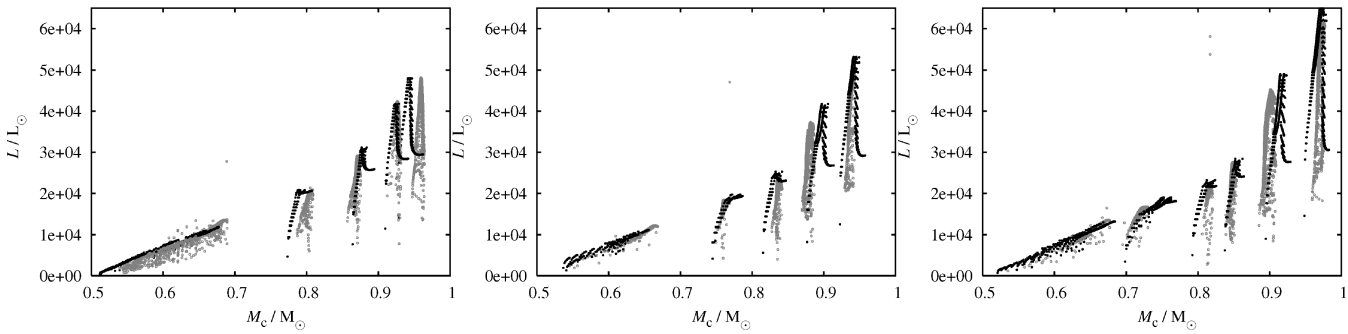

Figure 3. Luminosity versus core mass during the TPAGB phase for $Z = 0.02$ (left), 0.008 (centre) and 0.004 (right). The grey points are our full stellar evolution models, the black points our synthetic models with the same initial masses. Note that our full stellar evolution models include post-flash dips while the synthetic models do not. Models with core masses above about 0.8 $M_\odot$ show HBB.

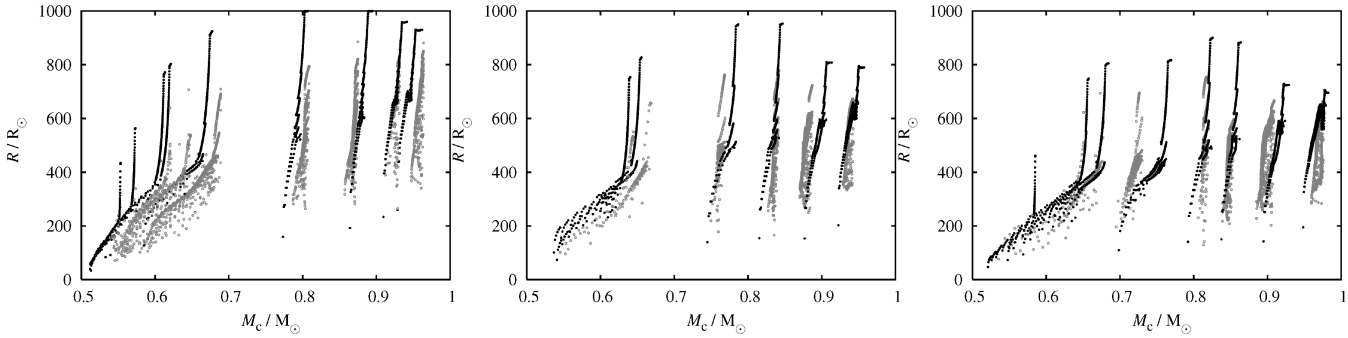

Figure 4. As Fig. 3 but for radius (prior to H02 small envelope corrections).

The fit takes the basic form $\log R \approx A \log L$ with corrections for envelope mass loss, metallicity and a small quadratic dependence on the core mass:

$$\log_{10}(f_R R/R_\odot) = a_{35} + 0.8l + b_{35}M_{c,1TP}/M_\odot + c_{35}M_{c,1TP}^2 + d_{35}\log_{10} Z + e_{35}Z, \quad (35)$$

where $l = \log_{10}(10^{-3}L/L_\odot)$ and $f_R = (M_{env}/M_{env,1TP})^{0.66}$ corrects for envelope removal. The complicated expression for the fit reflects the large changes in opacity in the stellar envelope over the evolution of the stars. As M_{env} tends to zero the radius diverges, so is capped at $10^3 R_\odot$. Fig. 4 shows the radius versus core mass from our full stellar evolution and synthetic models. Corrections are applied for small envelope mass as in H02 to facilitate a smooth transition from the AGB to the white dwarf cooling track.

3.3.4 Temperature at the base of the convective envelope

The temperature at the base of the convective envelope T_{bce} is the critical factor which governs the rate of HBB (see also Section 4.3.1). If the temperature is sufficiently high ($T_{bce} > T_{HBBmin} \approx 10^{7.5}$ K) it is possible that hydrogen burning occurs in the convective envelope of the star, altering the surface abundances. From our full stellar evolution models we see that the temperature rises quickly in these hot-bottom envelopes and then stays at a roughly constant value until the envelope mass becomes small. In order to model the HBB, a fit to the temperature in the burning zone is needed.

The base of the convective envelope is defined as the innermost point in the envelope at which the Schwarzschild condition for stability is no longer satisfied. The rise at the beginning of the AGB and the fall owing to envelope mass reduction at the end of the AGB are extremely difficult to parametrize, so we opt for simplicity and fit the maximum temperature over the lifetime of the star and modulate it for the rise and fall. The log of the temperature used in our nucleosynthesis code is then given by

$$\log_{10}(T_{bce}/K) = \log_{10}(T_{max}) f_{Trise} f_{Tdrop}, \quad (36)$$

where T_{max}, f_{Trise} and f_{Tdrop} are defined below.

The logarithm of the temperature maximum is fitted to

$$\log_{10}(T_{max}/K) = \min(6.0379 + a_{37}M_{env,0}/M_\odot + B(\zeta, M_{c,1TP}), 7.95), \quad (37)$$

where a_{37} is a constant and

$$B(\zeta, M_{c,1TP}) = \left(a_{38}\zeta^2 + b_{38}\zeta + c_{38}\right) \times \left[1 + d_{38}M_{c,1TP}/M_\odot + e_{38}(M_{c,1TP}/M_\odot)^2\right], \quad (38)$$

where $a_{38} \ldots e_{38}$ are constants. The maximum value of 7.95 is more a limitation of the HBB code (see Section 3.7) than an actual physical effect, but temperatures higher than this are only likely to be encountered in the most massive ($M = 6\ M_\odot$) and lowest metallicity ($Z \leqslant 0.004$) stars so the limit of 7.95 should not greatly affect the CNO yields.

The rise in temperature during the first few thermal pulses is modelled by a factor

$$f_{Trise} = 1.0 - \exp\left(-\frac{N}{N_{rise}}\right), \quad (39)$$

where N is the thermal pulse number and N_{rise} is a rather arbitrary constant, of the order of 1 for $M_i \approx 6\ M_\odot$, a few for $M_i \approx 5\ M_\odot$, about 20 for $M_i \approx 4\ M_\odot$ and possibly infinite for $M_i < 3.5\ M_\odot$

(because no HBB occurs in these stars, at least for $Z \geqslant 0.004$, although the $T_{\rm max} < T_{\rm HBB,min}$ condition will also prevent HBB). We use it as a free parameter in our nucleosynthesis model. It is important that HBB switches on quite suddenly, so even if $N_{\rm rise} \approx 6$, HBB is not fully active for about 15 pulses by which time $f_{\rm Trise} \approx 0.9$.

The drop in temperature owing to the decrease in envelope mass is taken care of by

$$f_{\rm Tdrop} = \left(\frac{M_{\rm env}}{M_{\rm env,1TP}} \right)^{\beta_{40}}, \tag{40}$$

where β_{40} is another free parameter which is quite uncertain. Fortunately $M_{\rm env}$ falls quickly during the superwind phase near the end of the AGB, so the uncertainty does not matter too much. We use a constant value $\beta_{40} = 0.02$ and this works well for most stars.

3.3.5 *Density at the base of the convective envelope*

The density ρ at the base of the convective envelope is not as important for nucleosynthesis as the temperature, but a reasonable value is required. We fit the maximum density over the TPAGB evolution of the star as a function of M_0 and Z:

$$\log_{10} \rho_{\rm max} = a_{41} + b_{41} \left(M_{\rm 1TP}^{c_{41}} / {\rm M}_\odot \right) + d_{41} \zeta. \tag{41}$$

This function is modulated by $f_{\rm Trise}$ and $M_{\rm env}/M_{\rm env,0}$ to give

$$\rho = \rho_{\rm max} f_{\rm Trise} \frac{M_{\rm env}}{M_{\rm env,1TP}} {\rm g\,cm^{-3}}. \tag{42}$$

This is a reasonable fit for $M_{\rm 1TP} > 3\ {\rm M}_\odot$ and models with $M_{\rm 1TP} < 3\ {\rm M}_\odot$ do not experience HBB.

3.4 Third dredge-up

The efficiency of third dredge-up is parametrized by

$$\lambda = \frac{\Delta M_{\rm dredge}}{\Delta M_{\rm H}}, \tag{43}$$

where $\Delta M_{\rm dredge}$ is the mass dredged up from the intershell region and $\Delta M_{\rm H}$ is the core mass increase owing to hydrogen burning during the previous interpulse period, so that over a whole interpulse period the core grows by $\Delta M_{\rm c} = \Delta M_{\rm H} - \Delta M_{\rm dredge} = (1 - \lambda)\Delta M_{\rm H}$. We calculate λ as function of mass and metallicity. The possibility of burning dredged-up material is also considered. Note that the fitting of λ to M is an approximation to the true, and unknown, form which would depend on $M_{\rm c}$ and $M_{\rm env}$.

The dredged-up material is instantaneously mixed with the convective envelope of the star. We note that there is a possibility of a degenerate thermal pulse in some stars (Frost et al. 1998); however, the effect is to increase the amount of ^{12}C dredged up by a factor of 4, making one degenerate pulse equivalent to four normal pulses. Frost et al. (1998) report degenerate thermal pulses in a $M = 5\ {\rm M}_\odot$, $Z = 0.004$ star which would also undergo many dozens of non-degenerate third dredge-up events, so the effect of one or two degenerate pulses is small compared with the effect of non-degenerate pulses. We neglect the phenomenon.

3.4.1 *Lambda parametrization and minimum mass for dredge-up*

K02 find third dredge-up for stars above a certain core mass $M_{\rm c}^{\rm min}$, a function of $M_{\rm i}$, Z and $M_{\rm sdu}$, where $M_{\rm sdu}$ is the mass above which second dredge-up occurs ($M_{\rm sdu} \approx 4\ {\rm M}_\odot$ for $Z = 0.02$ and $M_{\rm sdu} \approx 3.5\ {\rm M}_\odot$ for $Z = 0.004$). For $M < M_{\rm sdu}$ the minimum core mass is given by K02:

$$M_{\rm c}^{\rm min*}/{\rm M}_\odot = a_{44} + b_{44} M/{\rm M}_\odot + c_{44}(M/{\rm M}_\odot)^2 + {\rm d}_{44}(M/{\rm M}_\odot)^3. \tag{44}$$

We use the instantaneous mass M rather than $M_{\rm i}$ (as K02 do) to allow for effects of reduced envelope mass on λ, although without full stellar evolution models at this late stage of the TPAGB it is impossible to know whether this is entirely correct. For $M \geqslant M_{\rm sdu} - 0.5\ {\rm M}_\odot$, K02 found $M_{\rm c}^{\rm min} > 0.7\ {\rm M}_\odot$, so we set $M_{\rm c}^{\rm min} = M_{\rm c,1TP}$ as they do. Equation (44) diverges as M increases so is capped at $0.7\ {\rm M}_\odot$. A correction is subtracted for $Z < 0.004$ to force dredge-up in the low-metallicity models:

$$\Delta M_{\rm LZ} = -205.1 Z + 0.8205. \tag{45}$$

Finally we combine the above prescriptions, so for any M we set $M_{\rm c}^{\rm min}$ to

$$M_{\rm c}^{\rm min} = \max \left[M_{\rm c,1TP}, \min \left(0.7\,{\rm M}_\odot, M_{\rm c}^{\rm min*} - \Delta M_{\rm LZ} \right) \right]. \tag{46}$$

Below $M_{\rm c}^{\rm min}$, $\lambda = 0$. For $M_{\rm c} > M_{\rm c}^{\rm min}$, λ reaches an asymptotic value $\lambda_{\rm max}$ after $N_{\rm r}$ thermal pulses. $\lambda_{\rm max}$ is fitted with

$$\lambda_{\rm max} = \frac{a_{47} + b_{47} M/{\rm M}_\odot + c_{47}(M/{\rm M}_\odot)^3}{1 + d_{47}(M/{\rm M}_\odot)^3}, \tag{47}$$

with $a_{47} \ldots d_{47}$ functions of metallicity (K02). For $M \geqslant 3.0\ {\rm M}_\odot$, λ reaches a value of 0.8–0.9 with a slight metallicity dependence. At low metallicity dredge-up is efficient in lower mass stars, so for $Z \leqslant 0.004$ we use equation (47) with M artificially increased by an amount $60 \times (0.004 - Z)$.

We approximate the dependence on pulse number N by

$$\lambda(N) = \lambda_{\rm max}(1 - {\rm e}^{-N/N_{\rm r}}). \tag{48}$$

Table 5 of K02 lists appropriate values for $N_{\rm r}$ but there is no systematic variation that is easily fitted with a simple function. We use

$$N_{\rm r} = 4 + 3[1 - \exp(-M_{\rm 1TP}/{\rm M}_\odot)] \times [1 - a_{49} \exp(-Q_{49})], \tag{49}$$

where

$$Q_{49} = \left[(4 - M_{\rm 1TP}/{\rm M}_\odot + b_{49} Z)(4 - M_{\rm 1TP}/{\rm M}_\odot + c_{49} Z) \right] \tag{50}$$

which fits the dip in $N_{\rm r}$ around $M_{\rm 1TP} \approx 4\ {\rm M}_\odot$ (with slight metallicity dependence taken care of by b_{49} and c_{49}). This is well-behaved over the entire parameter space, and the difference between $M_{\rm 1TP}$ and M is irrelevant because this turn-on is only active for the first few pulses.

In Fig. 5 (left-hand panel) we show the temperature at the base of the convective envelope from our full stellar evolution models. Note that use of the Marigo, Girardi & Bressan (1999a) prescription for dredge-up above $\log_{10} T_{\rm bce} = 6.4$ would lead to dredge-up in all our stars. Also in Fig. 5 is a comparison of our $M_{\rm c}^{\rm min}$ with Marigo et al. (1999a)'s prescription (with $\log_{10} T_{\rm bce} = 6.4$) for solar metallicity. Even after calibration of our synthetic model by comparison to carbon star luminosity functions (see Section 5.1), which leads to a reduction in $M_{\rm c}^{\rm min}$, our synthetic models still have a slightly higher $M_{\rm c}^{\rm min}$ than Marigo et al. (1999a).

3.4.2 *Intershell abundances*

The abundances in the intershell region $X^{\rm i}$ are fitted to data taken from the final thermal pulse of the $Z = 0.02$ models and include a

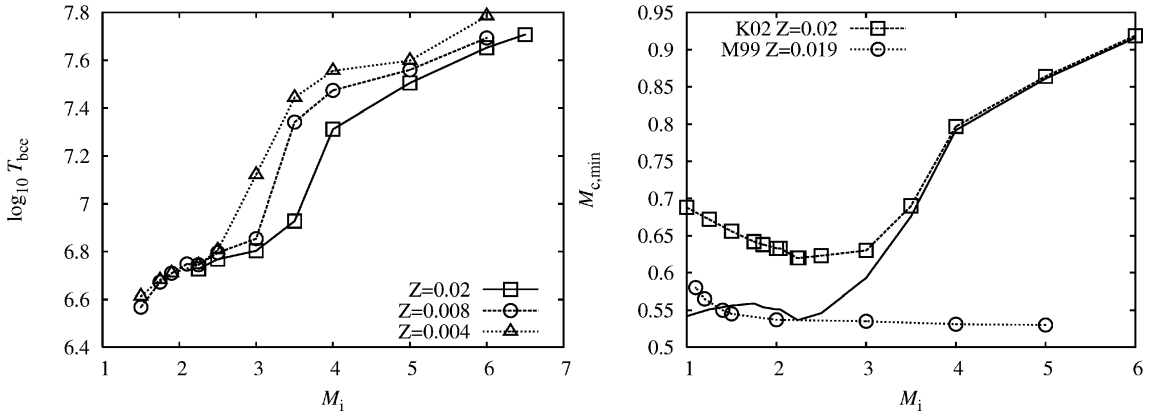

Figure 5. Left-hand panel: temperature at the base of the convective envelope at the first thermal pulse from our full stellar evolution models at various metallicities. Right-hand panel: $M_{\rm c}^{\rm min}$ from our full stellar evolution models (K02) and the model of Marigo et al. (1999a, M99). The solid line shows the core mass at the first thermal pulse (from K02).

dependence on $M_{1\rm TP}$. The $Z = 0.02$ values work well for all metallicities.

$$X^{\rm i}_{\rm He4} = \begin{cases} 0.636 & M_{1\rm TP} < 1.76\ {\rm M}_\odot, \\ a_{51} + b_{51} M_{1\rm TP} & \\ +c_{51} M_{1\rm TP}^2 + d_{51} M_{1\rm TP}^3 & M_{1\rm TP} \geqslant 1.76\ {\rm M}_\odot, \end{cases} \quad (51)$$

$$X^{\rm i}_{\rm O16} = \begin{cases} f^{\rm i}_{\rm O}(a_{52} + b_{52} M_{1\rm TP}) & M < 1.76\ {\rm M}_\odot, \\ f^{\rm i}_{\rm O}(c_{52} + d_{52} M_{1\rm TP} & \\ + e_{52} M_{1\rm TP}^2 + f_{52} M_{1\rm TP}^3) & M_{1\rm TP} \geqslant 1.76\ {\rm M}_\odot, \end{cases} \quad (52)$$

where $f^{\rm i}_{\rm O} = 1.5 - 1.3 \times 10^{-4} Z$ and

$$X^{\rm i}_{\rm C12} = \max\left(1, f^{\rm i}_{\rm O}\right) \times \left(a_{53} + b_{53} X^{\rm i}_{\rm He4}\right). \quad (53)$$

We calculate ^{22}Ne from the CNO abundance in the stellar envelope (envelope abundances given by X_i) just prior to dredge-up. All CNO is burned to ^{14}N which in turn is burned to ^{22}Ne:

$$X^{\rm i}_{\rm Ne22} = 22 \left(\frac{X_{\rm C12}}{12} + \frac{X_{\rm C13}}{13} + \frac{X_{\rm N14}}{14} + \frac{X_{\rm N15}}{15} + \frac{X_{\rm O16}}{16} + \frac{X_{\rm O17}}{17} \right) + X_{\rm Ne22}. \quad (54)$$

All other isotopes are set to zero in the intershell region and the abundances are renormalized such that their sum is 1.0. The above fits give typical intershell abundances (for a solar metallicity, 5-$M_\odot$ model) of 74 per cent ^{4}He, 23 per cent ^{12}C, 0.5 per cent ^{16}O and 2 per cent ^{22}Ne.

Our full stellar evolution models do not obtain high values of intershell ^{16}O such as the 2 per cent reported by Boothroyd & Sackmann (1988). There is some debate on the exact composition in the intershell region. The inclusion of diffusive overshooting (Herwig 2000) increases the abundance of ^{12}C and ^{16}O at the expense of ^{4}He.

3.4.3 Dredge-up of the hydrogen-burning shell

Others (notably GdJ93, equation 35) include nuclear burning of third dredge-up material as well as envelope burning (Section 3.7 below). The reason for this is that material brought up by third dredge-up is preferentially exposed to high temperatures at the base of the convective envelope. Our full stellar evolution models do not show this phenomenon although, in our low-metallicity models, there is dredge-up of ^{13}C and ^{14}N that leads to a similar effect which cannot possibly result from helium burning. These isotopes are enhanced in the envelope by dredge-up of material previously in the hydrogen-burning shell (burnt during the interpulse period) but not mixed into the intershell convective zone.

We account for this by burning a fraction $f_{\rm DUP}$ of $\Delta M_{\rm dredge}$ for a fraction of the interpulse period $f_{\rm burn,DUP}$ and at the temperature and density at the base of the envelope (extrapolated from equations 37 and 41). The hydrogen abundance of the material to be burned is set to the envelope hydrogen abundance (even though it may be somewhat lower due to interpulse hydrogen shell burning). Because $f_{\rm DUP}$ and $f_{\rm burn,DUP}$ are fitted to the full evolution models, any problems are circumvented by the calibration. The burning algorithm is described in Section 3.7.1 and is the same algorithm as used for HBB. The hydrogen-burned material is immediately mixed with both the helium-burned intershell material and the whole convective envelope to give the post-third dredge-up envelope abundances.

Note that when normal HBB occurs it is the dominant burning mechanism. At metallicity greater than 0.004 the change of ^{13}C and ^{14}N in the envelope due to the dredge-up of the H-burning shell is negligible compared with the abundance of ^{13}C and ^{14}N already in the envelope. The model used here is only approximate (and does not reflect the actual hydrogen-burning process), and we hope to improve upon it soon when more low-Z full evolution models become available.

3.5 Core growth during the interpulse period

Between pulses the hydrogen-deficient core grows owing to (radiative) hydrogen burning. The luminosity is due mainly to H burning and so can be used to calculate the change in core mass during any time-step:

$$\Delta M_{\rm c} = \min(L, L_{\rm max}) Q \delta t, \quad (55)$$

where L is the luminosity, δt is the time-step, and Q is the effective nuclear burning efficiency. L is capped at $L_{\rm max} = 3.0 \times 10^4\ {\rm L}_\odot$ because an increase in core size beyond this rate is not seen in our full stellar evolution models. Q is set to $1.585 \times 10^{-11}\ {\rm M}_\odot\ {\rm L}_\odot^{-1}\ {\rm yr}^{-1}$ as fitted to our full stellar evolution models (this value takes into account both hydrogen burning and helium burning, as well as gravitational effects and compositional effects such as a non-uniform hydrogen mass fraction in the shell) which compares reasonably to the values $1.27 \times 10^{-11}\ {\rm M}_\odot\ {\rm L}_\odot^{-1}\ {\rm yr}^{-1}$ in Hurley

et al. (2000) and 1.02×10^{-11} $M_\odot$ $L_\odot^{-1}$ yr^{-1} in Wagenhuber & Groenewegen (1998). No X_{H1} dependence is evident in our full stellar evolution models.

3.6 Wind loss prescription

To compare our synthetic model with our full stellar evolution models, the same wind loss prescription is used (section 2 of K02). Before the giant branch the mass-loss rate $\dot{M}$ is negligible (we set $\dot{M} = 0$ in both our synthetic model and full stellar evolution models). On the giant branch the formula of Kudritzki & Reimers (1978) with $\eta = 0.4$ is used. On the EAGB and TPAGB the mass-loss rate is according to VW93, without the correction for masses above 2.5 $M_\odot$, where

$$\log_{10}(\dot{M}/M_\odot\ yr^{-1}) = -11.4 + 0.0125(P/d), \tag{56}$$

where P is the Mira pulsation period given by

$$\log_{10}(P/d) = -2.07 - 0.9\log_{10}(M/M_\odot) + 1.94\log_{10}(R/R_\odot). \tag{57}$$

A typical mass-loss rate is then about 10^{-9} $M_\odot$ yr^{-1} for a 1.9 $-$ $M_\odot$, $Z = 0.008$ star (a typical carbon star mass, with $L \approx 5 \times 10^3 L_\odot$, $R \approx 200$ $R_\odot$ and $P \approx 200$ d) prior to superwind. This is a little low compared with observations (e.g. Wallerstein & Knapp 1998), although higher mass stars have significantly higher rates (e.g. $\dot{M} \approx 4 \times 10^{-7}$ $M_\odot$ yr^{-1} for $M = 6$ $M_\odot$, $Z = 0.02$) and as Wallerstein & Knapp (1998) point out it is more difficult to observe AGB stars with low mass-loss rates so there is some observational bias.

On the TPAGB and for $P \geqslant P_{max}$ the rate in equation (56) is truncated (if necessary) to a superwind given by

$$\dot{M} = \frac{L}{c v_{exp}}, \tag{58}$$

where c is the speed of light and v_{exp} is the expansion velocity of the wind (VW93) given by

$$v_{exp} = \min\left[(-13.5 + 0.056 P_{max}/d),\ 15\right] km s^{-1}. \tag{59}$$

Our full stellar evolution models have $P_{max} = 500$ d and we use this in our standard synthetic model. The superwind mass-loss rate is much greater than the rate given in equation (56), and leads to a very quick end for the star and probably results in a planetary nebula. For the 1.9-$M_\odot$, $Z = 0.008$ star a typical superwind mass-loss rate is about $10^{-5} M_\odot$ yr^{-1}; this is typical for all our TPAGB stars and agrees reasonably with observations (Wallerstein & Knapp 1998).

Note that the radius used in the above prescription is that of equation (35) without the small-envelope correction of H02. This is because the corrected radius drops as the envelope mass becomes small, leading to a small wind-loss rate – the use of the fitted radius (which diverges as the envelope becomes small) ensures that the envelope is lost rapidly at the end of the AGB phase.

Table 4. Reactions used in the rapid CNO bi-cycle. The left-hand column gives the reaction number used in the text, i, and the right-hand column shows the corresponding nuclear reaction.

i	Reaction
12	$^{12}C + {}^1H \rightarrow {}^{13}N + \gamma$
13	$^{13}C + {}^1H \rightarrow {}^{14}N + \gamma$
14	$^{14}N + {}^1H \rightarrow {}^{15}O + \gamma$
16	$^{16}O + {}^1H \rightarrow {}^{17}F + \gamma$
17	$^{17}O + {}^1H \rightarrow {}^{14}N + {}^4He$

3.7 Hot-bottom burning

If the hydrogen envelope of an AGB star is sufficiently massive, the hydrogen-burning shell can extend into the convective region, a process known as hot-bottom burning (HBB). We deal with HBB by burning a fraction of the convective envelope f_{HBB} for a fraction of the time-step period f_{burn} at the temperature and density as fitted in Sections 3.3.4 and 3.3.5. The burned fraction is mixed with the rest of the convective envelope at the end of the time-step (usually coincident with the end of the interpulse period). The validity of this approach is discussed in Section 3.7.2. We burn only CNO, but HBB affects other elements via the NeNa and MgAl chains (see Karakas & Lattanzio 2003) as well as lithium via pp-burning. These are difficult problems which are being worked on but are outside the scope of this paper. HBB also depends on the mixing-length parameter because the base of the convective envelope is linked to superadiabatic layers near the surface by an adiabat; however, we ignore this and use a fixed value $\alpha = 1.75$.

3.7.1 Clayton's CNO cycle

We burn the CNO elements according to Clayton's CNO bi-cycle (Clayton 1983). He claims this is accurate to 1 per cent for the temperature range we are considering ($\log_{10}T/K < 8$), and this was confirmed by GdJ93 who used a similar approach. We calibrate out any errors (see Section 4). It is much faster than solving the differential equations of a complete nuclear reaction network.

The CNO cycle can be simplified from the full set of differential equations if ^{13}N, ^{15}N, ^{15}O and ^{17}F are in equilibrium. The cycle then splits into two, the CN cycle and the ON cycle, with branching ratios $\alpha_{CN} = 1 - \gamma$ and $\gamma \simeq 7 \times 10^{-4}$ respectively (Angulo et al. 1999). The small value of γ reflects the fact that the time-scales in the ON cycle are many thousands of times those required to bring the CN cycle into equilibrium so we can treat the cycles separately.

The CN cycle equations, with $\alpha_{CN} = 1$, become

$$\frac{d}{dt}\begin{bmatrix} {}^{12}C \\ {}^{13}C \\ {}^{14}N \end{bmatrix} = \begin{bmatrix} -1/\tau_{12} & 0 & 1/\tau_{14} \\ 1/\tau_{12} & -1/\tau_{13} & 0 \\ 0 & 1/\tau_{13} & -1/\tau_{14} \end{bmatrix} \begin{bmatrix} {}^{12}C \\ {}^{13}C \\ {}^{14}N \end{bmatrix} \tag{60}$$

which is of the form $\frac{d}{dt}\boldsymbol{U} = \Lambda\boldsymbol{U}$. Eigenvalues λ_i are given by $\Lambda\boldsymbol{U}_i = \lambda_i \boldsymbol{U}_i$ (no sum over i) and $\boldsymbol{U}$ is a linear combination of the eigenvectors $\boldsymbol{U}_i$, so

$$\boldsymbol{U}(t) = Ae^{\lambda_1 t}\boldsymbol{U}_1 + Be^{\lambda_2 t}\boldsymbol{U}_2 + Ce^{\lambda_3 t}\boldsymbol{U}_3. \tag{61}$$

The time-scales τ_i are defined by

$$\tau_i = (\langle\sigma v\rangle_i X_{H1})^{-1}, \tag{62}$$

where $\langle\sigma v\rangle_i$ is the velocity-averaged cross-section for the appropriate reaction i (see Table 4). The rate of change of each isotope (equation 60) is proportional to the cross-section, the hydrogen density and the isotope density.

The method of solution for equation (60) is found in Clayton (1983) (but beware the typographical error!). The time-step δt is substituted for t in equation (61) to calculate the abundances at the end of the current time-step.

The ON cycle equations are identical to the CN cycle, with ^{12}C, ^{13}C and ^{14}N replaced by ^{14}N, ^{16}O and ^{17}O and with appropriate τ_i (see Table 4 and Clayton 1983). The minor species ^{15}N and ^{17}O are assumed to be in equilibrium. Any ^{17}F produced is assumed to decay immediately to ^{17}O ($\tau_{1/2} \approx 65$ s).

For short burning times ($\delta t < \tau_{12}$) only the CN part of the cycle is necessary. For longer times, the CN cycle is burned to equilibrium

before the ON cycle is activated. Even in the most massive AGB stars undergoing vigorous HBB, $X_{\rm O16}$ does not change much so the ON cycle never approaches equilibrium. Nuclear reaction rates are taken from the formulae in the NACRE compilation (Angulo et al. 1999) except the beta decay constants which are taken from the compilation of Tuli (2000). The rates compare well to table 5.3 (p. 393) of Clayton (1983).

3.7.2 Thin shell burning versus whole envelope burning approximation

Between pulses the convective envelope of an AGB star turns over many thousands of times. It is impossible to model this using little CPU time because the burn → mix → burn → mix ... process is computationally expensive, especially if the code is to be extended to more isotopes than just ^{1}H, ^{4}He and CNO. Given the uncertainties involved in convective mixing and local mixing at the base of the envelope, it is simpler and preferable to approximate the burning (many times) of a thin HBB layer at the base of the convective envelope with a single burning of a larger portion of the envelope.

This can be justified by considering the size of the HBB region. For a 5-$M_\odot$ star d $\log_{10}(T/{\rm K})/{\rm d}m$ at the base of the envelope is typically $3 \times 10^3 {\rm M}_\odot^{-1}$. HBB ceases at $\log_{10}(T/{\rm K}) \approx 7.6$ and the temperature at the base of the envelope is typically $\log_{10}(T/{\rm K}) \approx 8$ for most of the TPAGB. So $\Delta M_{\rm HBB} \approx 10^{-4} {\rm M}_\odot$. This is much smaller than the size of the convective envelope (about 4 $M_\odot$ for a 5-$M_\odot$ star), so the HBB shell can be considered as thin.

When the thin HBB shell is burned and then mixed into the envelope the abundances in the envelope are essentially unchanged. Only once a significant number of mixings (of the order $M_{\rm env}/\Delta M_{\rm HBB}$) have occurred will the envelope abundances change noticeably, so in our approximation we burn a fraction of the envelope, $f_{\rm HBB}$, for a fraction of the interpulse period time $f_{\rm burn}$ and fit $f_{\rm HBB}$ and $f_{\rm burn}$ to our full stellar evolution models. In reality, some parts of the envelope burn more than once but this is absorbed into the calibration of $f_{\rm HBB}$. The burned shell and the rest of the envelope are mixed at the end of the time-step.

To calibrate the model we allow mixing 10 times per interpulse period so the shape of the abundances versus time profiles between pulses can be observed. The code is designed so that the result is identical to that obtained if there is only one mixing per interpulse in the way that the code is expected to be used in population synthesis runs.

Note that this technique differs from that of GdJ93 where the average abundance rather than the final abundance between time 0 and $f_{\rm burn}\tau_{\rm ip}$ is mixed into the envelope.

4 HBB CALIBRATION AND COMPARISON OF SYNTHETIC MODELS WITH FULL EVOLUTIONARY MODELS

The free parameters,

(i) $f_{\rm HBB}$ – the fraction of the envelope of the star that is burned in the HBB shell,

(ii) $f_{\rm burn}$ – the fraction of the interpulse period for which the HBB shell burns,

(iii) $f_{\rm DUP}$ – the fraction of the dredged-up material that is hydrogen-burned before being mixed into the envelope to simulate dredge-up of the hydrogen shell in low-Z stars,

(iv) $f_{\rm DUP,burn}$ – the fraction of the interpulse period for which the dredged-up material is burned, and

Table 5. Burning time $10^6 f_{\rm burn}$ as a fraction of the interpulse period for different masses and metallicities. The first row of numbers for each Z are the ranges narrowed down by the MC runs. The second row of numbers are used to fit a relation to $M_{\rm 1TP}$ and Z. $f_{\rm burn} = 0$ for $M_{\rm 1TP} < 3.5$ M$_\odot$.

$Z \downarrow M_{\rm 1TP}/{\rm M}_\odot \rightarrow$	3.5	4.0	5.0	6.0	6.5
0.02	–	–	0.1–0.5	0.5–0.6	0.4–1.0
			0.3	0.55	0.7
0.008	0	<0.2	0.6–1.0	0.8–1.0	
	0	0.1	0.8	0.9	
0.004	0	0.15–0.5	0.5–1.0	0.8–10	
	0	0.3	0.75	0.9	

(v) $N_{\rm rise}$ – the factor used to define how quickly the HBB temperature reaches $T_{\rm max}$,

are to be calibrated to our full stellar evolution models.

Previous authors (e.g. GdJ93) have used constant values for $f_{\rm HBB}$, $f_{\rm burn}$, $f_{\rm DUP}$ and $f_{\rm DUP,burn}$, with a different prescription for the temperature (not requiring $N_{\rm rise}$). Here we assume that these values differ for each star, so we attempt to parameterize them in terms of $M_{\rm 1TP}$ and Z. Often we quote $10^6 f_{\rm burn}$ instead of $f_{\rm burn}$ because $f_{\rm burn} \lesssim 10^{-6}$.

4.1 Calibration method

A Monte Carlo (MC) method is used to test the above free parameters with ranges $0.0 < f_{\rm HBB} < 1.0$, $0.0 < 10^6 f_{\rm burn} < 10.0$ and $0 < N_{\rm Trise} < 20$. $f_{\rm DUP}$ and $f_{\rm DUP,burn}$ are chosen to be zero and are only increased when necessary.

A weighted sum of squares is constructed from our full stellar evolution model nucleosynthesis data versus the corresponding synthetic model nucleosynthesis results to enable comparison between MC model runs. A score $= (\sum_i w_i s_i)^{-1}$ is defined such that higher numbers mean a better fit where the weights are $w_i = (w_{\rm C12}, w_{\rm C13}, w_{\rm N14}, w_{\rm O16}, w_{\rm C/O}, w_{\rm C12/C13}) = (1, 10, 1, 1, 5, 5)$ and s_i is the sum of squares difference between our full stellar evolution and synthetic models for the isotope (or ratio) i. The ratios $X_{\rm C12}/X_{\rm C13}$ and $X_{\rm C}/X_{\rm O}$ are weighted preferentially because these are important observed nucleosynthetic constraints on AGB stars. ^{13}C is also boosted because its abundance is small. 1D slices and 2D projections of the resulting parameter space are then examined and compared with the best fit obtained by this method. Human intervention comes last but proves invaluable when trying to fit the details. Appendix B[7] contains the details of the calibration results.

4.2 Free parameter Heaven or Hell

The results of the MC runs for each star are shown in Tables 5, 6 and 7. Ranges are given when the MC technique cannot distinguish a unique solution. In such cases we choose a value that aids the fit of the free parameter to $M_{\rm 1TP}$ and Z or such that $10^6 f_{\rm burn} \approx f_{\rm HBB}$. The chosen value is shown under the range. If the value is '–' then there is no HBB so $f_{\rm DUP} = f_{\rm burn} = 0.0$. Where no value is given there is no full stellar evolution model with which to compare. It is not possible to use the best MC values for every star because there is too much non-systematic scatter.

[7] http://www.blackwellpublishing.com/products/journals/suppmat/mnr/mnr7446/mnr7446sm.htm

Table 6. Envelope mass fraction exposed to HBB, $f_{\rm HBB}$, for different masses and metallicities. The first row of numbers for each Z are the ranges narrowed down by the MC runs. The second row of numbers are used to fit a relation to $M_{\rm 1TP}$ and Z. $f_{\rm HBB}=0$ for $M_{\rm 1TP}<3.5\,{\rm M}_\odot$.

$Z\downarrow M_{\rm 1TP}/{\rm M}_\odot\rightarrow$	3.5	4.0	5.0	6.0	6.5
0.02	–	–	0.1–0.4	0.65	0.3–1.0
			0.25	0.65	0.7
0.008	0	0.1–0.2	0.4–1.0	0.7–1.0	
	0	0.15	0.7	0.85	
0.004	<0.1	0.1–0.5	0.8–1.0	0.75–1.0	
	0.1	0.3	0.9	0.85	

Table 7. Temperature rise factor $N_{\rm rise}$ for different masses and metallicities. The first row of numbers for each Z are the ranges narrowed down by the MC runs. The second row of numbers are used to fit a relation to $M_{\rm 1TP}$ and Z. $N_{\rm rise}$ is undefined for $M_{\rm 1TP}<3.5\,{\rm M}_\odot$ (because $f_{\rm burn}=f_{\rm HBB}=0$).

$Z\downarrow M_{\rm 1TP}/{\rm M}_\odot\rightarrow$	3.5	4.0	5.0	6.0	6.5
0.02	–	–	∼3	<1	1–2
			3	0.5	1.5
0.008	⩾6	∼6	∼2.5	∼2	
	6	6	2.5	2	
0.004	∼6	∼3	<2	<1	
	6	3	2	1	

The values for $f_{\rm HBB}$ and $f_{\rm burn}$ are zero for $M_{\rm 1TP}<3.5\,{\rm M}_\odot$ with a step up to about 0.9 at $M_{\rm 1TP}\approx4.5\,{\rm M}_\odot$ and a slight metallicity dependence. These can be reasonably well fitted to a function f_{63} similar to a Fermi function:

$$f_{63}=\frac{(a_{63}Z+b_{63})}{1+(c_{63}Z+d_{63})^{(e_{63}Z+g_{63}-M_{\rm 1TP}/{\rm M}_\odot)}}. \tag{63}$$

The f_{63} parameter for $f_{\rm HBB}$ or $10^6 f_{\rm burn}$ is then given by $\max(f_{63}, 0.0)$.

$N_{\rm rise}$ is fitted to a quadratic in $M_{\rm 1TP}$ and $z=\min({\rm Z}, 0.02)$:

$$N_{\rm rise}=\max[a_{64}(M_{\rm 1TP}/{\rm M}_\odot)^2+b_{64}(M_{\rm 1TP}/{\rm M}_\odot)+c_{64}z+d_{64}z^2+e_{64}, 0]. \tag{64}$$

The maximum value for Z is necessary to maintain the behaviour of the function at higher metallicity. Equation (64) reaches a minimum value at around $M_{\rm 1TP}=6\,{\rm M}_\odot$ and is assumed to be valid for masses higher than this.

For $Z<0.004$ we include some immediate burning of dredge-up material.

4.3 Sensitivity to $f_{\rm HBB}$, $f_{\rm burn}$ and $N_{\rm rise}$

With the model described above and an appropriate choice of $f_{\rm HBB}$, $f_{\rm burn}$ and $N_{\rm rise}$, it is possible to match our full stellar evolution models to our synthetic models quite accurately. Problems occur with the fitted values of $f_{\rm HBB}$, $f_{\rm burn}$ and $N_{\rm rise}$ because minor deviations in the fit of the free parameters produce very different output (the sensitivity does not help us to pin down unique values for $f_{\rm burn}$ and $f_{\rm HBB}$ because of their inherent degeneracy). For example, if $N_{\rm rise}$ is too small then ^{13}C rises and falls too early in the $M_{\rm i}=6\,{\rm M}_\odot$ stars. If $f_{\rm burn}$ is even slightly too small then the ON cycle does not get switched on.[8] If $f_{\rm burn}$ is slightly too large then more ^{14}N is produced at the expense of ^{12}C and ^{13}C. A slight rise in $f_{\rm HBB}$ causes a large rise in HBB products, especially ^{14}N. The sensitivity to $f_{\rm HBB}$ and $f_{\rm burn}$ is compounded when both are erroneous in the same direction.

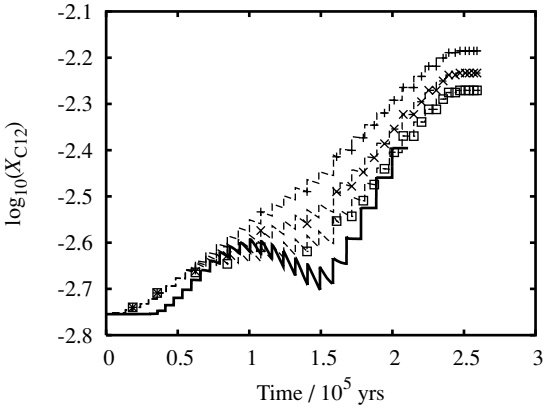

Figure 6. ^{12}C abundance versus time for $M_{\rm i}=5\,{\rm M}_\odot$, $Z=0.02$ with varying $f_{\rm HBB}=f_{\rm HBB}^{\rm fit}+\Delta f$, with $-0.13<\Delta f<0.13$. The fitted value of $f_{\rm HBB}$ is slightly wrong, but this only gives a maximum error of 0.15. The solid line is the full stellar evolution model; the other three lines are $\Delta f=-0.13$, 0 and +0.13 denoted with pluses, crosses and open squares respectively.

A change to $f_{\rm HBB}$ affects the ^{12}C surface abundance evolution for $M_{\rm i}=5\,{\rm M}_\odot$, $Z=0.02$ (see Fig. 6). An increased $f_{\rm HBB}$ better fits the drop in ^{12}C which occurs when HBB sets in, but by the end of the evolution the surface abundances are not very different. At most $X_{\rm C12}$ is wrong by a factor of 1.4 at any point over the entire evolution, while overall it changes by a factor of *5*. Final ^{13}C and ^{14}N have a similar scatter in $\log_{10}X$ of about 0.15. These effects are hardly visible in the case of the $M_{\rm i}=6\,{\rm M}_\odot$, $Z=0.02$ star and, because no burning occurs at all at $M_{\rm i}/{\rm M}_\odot=4$, it is only in the $M_{\rm i}/{\rm M}_\odot\approx4.5$–5 transition zone that we have to worry about this.

Alteration of the burning time, $f_{\rm burn}$, has essentially the same effect as a similar change in $f_{\rm HBB}$ with the exception of oxygen which is burned in the ON cycle when $f_{\rm burn}$ is long enough. The amount of ^{16}O burned for $M_{\rm i}=6\,{\rm M}_\odot$, $Z=0.02$ is very small in our full stellar evolution models ($\Delta\log_{10}X_{\rm O16}=-0.04$). This is about twice the size of the spread with $\Delta f_{\rm burn}=\pm0.13$ so we should not read too much into this. Significant oxygen burning occurs for $M_{\rm i}=6\,{\rm M}_\odot$, $Z=0.004$ but the standard model deals quite well with this (see Fig. 7). The carbon and nitrogen abundances are weakly affected at $M_{\rm i}=6\,{\rm M}_\odot$ but at the transition mass ($M_{\rm i}=5\,{\rm M}_\odot$ for $Z=0.02$, $M_{\rm i}=4\,{\rm M}_\odot$ for $Z=0.004$) the surface abundance is sensitive to $f_{\rm burn}$.

In summary, stars in the zone of transition between non-HBB and HBB ($M_{\rm i}=4\,{\rm M}_\odot$ for $Z=0.004$, $M_{\rm i}=5\,{\rm M}_\odot$ for $Z=0.02$) are the most troublesome when it comes to errors in the fit to $f_{\rm HBB}$ and $f_{\rm burn}$. However, this transition is quite sharp, so not too many stars in a population would have the wrong surface abundances.

[8] This is not a huge problem (except for $M_{\rm i}>6\,{\rm M}_\odot$) because most stars do not change their surface oxygen abundance significantly over their lifetime. For $M_{\rm i}>6\,{\rm M}_\odot$ and low Z this could be a source of worry.

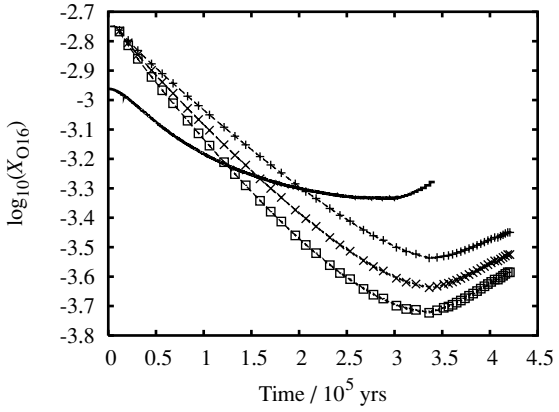

Figure 7. ^{16}O abundance versus time for the $M_{\rm i} = 6$ M$_\odot$, $Z = 0.004$ models, with $f_{\rm burn}$ set to $f_{\rm burn}^{\rm fit} + \Delta f$, where $-0.13 < \Delta f < 0.13$. Our standard synthetic model ($\Delta f = 0$) does a reasonable job of reproducing the full stellar evolution model. The solid line is the full stellar evolution model; the others from top to bottom are $\Delta f = -0.13$, 0 and $+0.13$ denoted with pluses, crosses and open squares respectively.

4.3.1 Temperature sensitivity

If the fit to the temperature of the HBB layer (Section 3.3.4) is allowed to vary even by a tiny amount, while the other free parameters are kept constant, CNO element production varies significantly. To show this, $\log_{10} T_{\rm max}$ is allowed to vary from the fitted value by a factor of $0.98 < f_T < 1.02$, just 2 per cent variations (5 per cent in $T_{\rm max}$), and the abundance versus time profiles are compared for the case $M_{\rm i} = 6$ M$_\odot$, $Z = 0.02$ which would ordinarily undergo large amounts of HBB (see Fig. 8). We do not always expect $f_T = 1.00$ to be the best fit because in reality the HBB layer has a temperature profile while in our synthetic model it does not. Note that the $\log_{10} T_{\rm max}$ limit of 7.95 has been disabled for these tests, leading to numerical problems due to imaginary eigenvalues at $f_T = 1.02$.

(i) The final ^{12}C is not greatly affected by temperature changes but $f_T = 0.98$ effectively switches off HBB. Paradoxically $f_T = 1.02$ burns less ^{12}C than $f_T = 1.01$ during most of the evolution. This is because $f_T = 1.02$ puts the temperature above the $\log_{10}(T/{\rm K}) = 7.95$ limit of applicability of the burning code. The best fit is for $f_T = 1.0$.

(ii) ^{13}C is affected in a more subtle way. At low temperature more ^{13}C is produced by incomplete CNO cycling. At the higher temperatures this ^{13}C is converted to ^{14}N. The final abundances for $f_T > 1.0$ are all similar because CN equilibrium is achieved, while for $f_T < 1.00$ there has not been enough conversion of ^{13}C to ^{14}N. Again $f_T = 1.00$ is the best fit.

(iii) The log of the final surface abundance of nitrogen varies from -2.55 at $f_T = 0.98$ (the same as the abundance at the start of the TPAGB) to -1.85 at $f_T = 1.02$. The best fit is $f_T = 1.01$ although $f_T = 1.00$ is not too bad. For $f_T \geqslant$

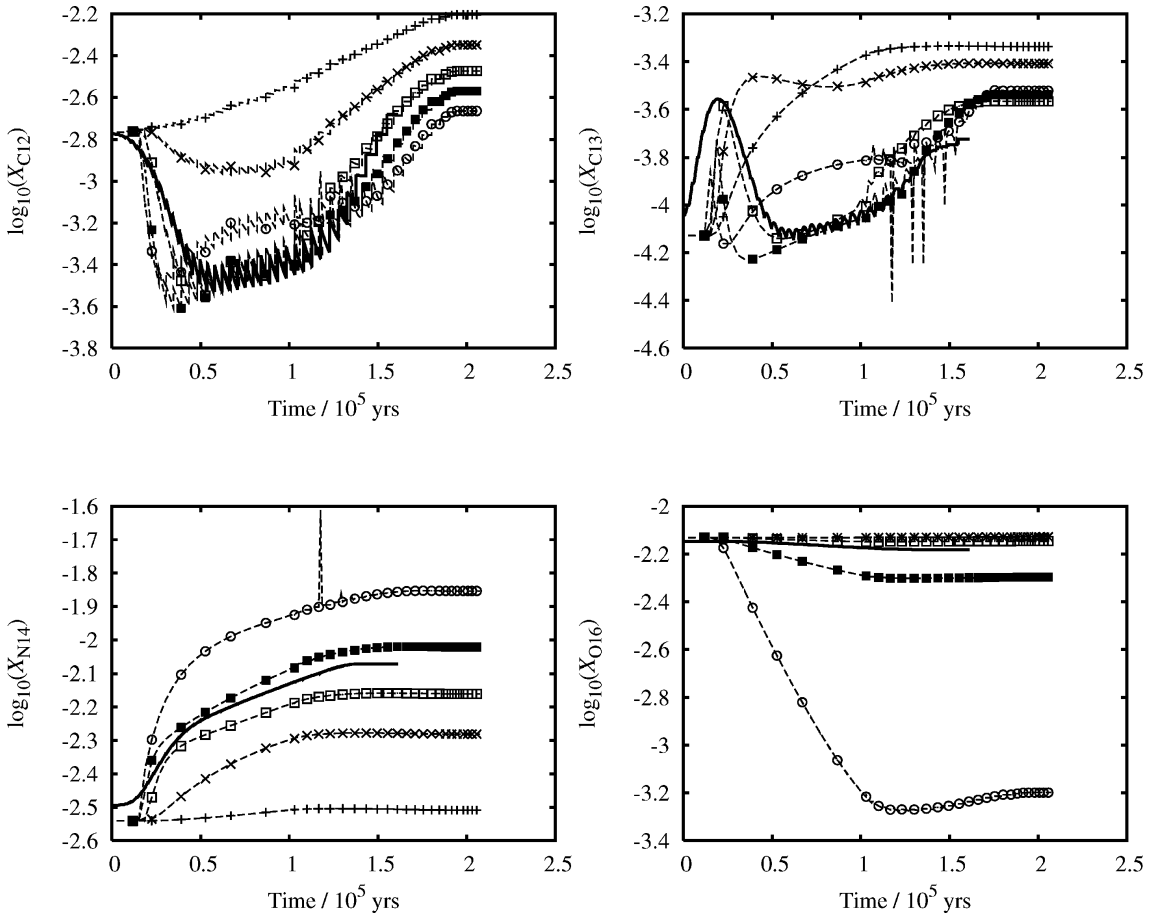

Figure 8. ^{12}C, ^{13}C, ^{14}N and ^{16}O surface abundances versus time for $M_{\rm i} = 6$ M$_\odot$, $Z = 0.02$ with varying temperature factor $0.98 < f_T < 1.02$. The solid line is our full stellar evolution model. The dashed lines represent $f_T = 0.98$ to 1.02 in 0.01 increments, from top to bottom (pluses, crosses, open squares, filled squares and open circles respectively). See text for details.

1.01 nitrogen abundances are high because of excessive ON cycling.

(iv) Out of all the CNO elements the surface oxygen abundance varies the most with temperature. For $f_T \leqslant 1.00$ there is little change in oxygen abundance, just as in our full stellar evolution models. An increase in the value of f_T to just 1.02 causes the surface oxygen abundance to drop by a factor of 10. This is not seen in our full stellar evolution models, so a value of $f_T = 1.00$ is certainly justified while $f_T = 1.01$ also gives too large a drop.

4.3.2 Dangerous interpolations and extrapolations

The TPAGB code is designed to be inserted into the rapid stellar evolution code, which deals with both single and binary stars for $0.1 \leqslant M_\mathrm{i}/\mathrm{M}_\odot \leqslant 100.0$ and $0.0001 \leqslant Z \leqslant 0.03$. This means that the expressions in the TPAGB code, developed here for $1 \lesssim M_\mathrm{i}/\mathrm{M}_\odot \lesssim 6.5$ and $0.004 \leqslant Z \leqslant 0.02$, or $M_\mathrm{i} \leqslant 2.25\ \mathrm{M}_\odot$, $Z = 0.0001$, must be interpolated over a factor of 40 in Z, or extrapolated beyond $Z = 0.004$ for $M \gtrsim 2.5\ \mathrm{M}_\odot$, into regimes where they have not been fitted to full stellar evolution models. Our expressions are designed to give sensible results when extrapolated or interpolated to low metallicity, but we have no way to tell if the results are correct.

5 DREDGE-UP CALIBRATION AND COMPARISON WITH OBSERVATIONS

5.1 Carbon stars

The carbon star luminosity function (CSLF) is defined as the number of carbon stars per unit bolometric magnitude for a particular population, i.e. it is a probability density function. We model a population of stars in the mass range $0.5 \leqslant M_\mathrm{i}/\mathrm{M}_\odot \leqslant 8.0$ where the probability for each star is taken from the initial mass function of Kroupa, Tout & Gilmore (1993) (KTG93, see also Appendix A7) and we assume a constant star formation rate. Results are compared with the Large Magellanic Cloud (LMC) ($Z = 0.008$) and Small Magellanic Cloud (SMC) ($Z = 0.004$) data taken from Groenewegen (2002) (2002; see also Groenewegen 1999). The theoretical distributions are binned identically to the observed data in 0.25-mag bins. All distributions are normalized such that the integrated probability is 1.0 (so are independent of the star formation rate if we assume it is constant). Because the bin widths are fixed, the probability density is directly proportional to the probability per bin (i.e. the number of stars per bin) so is directly compared to the (suitably normalized) observations.

It turns out that to fit the dim carbon stars with bolometric magnitude less than -3 we have to introduce a correction to the luminosity to deal with post-flash minima. This is a factor of the form

$$f_L = 1 - 0.5 \times \min\left[1, \exp\left(-3\frac{\tau}{\tau_\mathrm{ip}}\right)\right], \tag{65}$$

which is activated for the first 10 pulses to mimic the full evolution models. After about 10 pulses the luminosity dip lasts for a short time and is not of large enough magnitude to contribute to the dim CSLF tail (the maximum dip seen in the full evolution models is a factor of $0.5L$ equivalent to 0.75 mag). Extending the dip to all pulses does not significantly change the model CSLF of either the SMC or the LMC. The dimmest of carbon stars with magnitude about -3 cannot be fitted at all because they are probably extrinsic carbon stars in binary systems (Izzard & Tout 2004). Note that in order to resolve the dips the time-step is reduced to at most one-tenth of the interpulse period.

5.2 Modification of dredge-up parameters

The problem with the CSLF is that detailed models predict a distribution of stars that is too bright. Despite the addition of luminosity dips or changes in the wind-loss prescription, it proves impossible (with this model) to reproduce such low-luminosity carbon stars. The accepted interpretation, which we are forced to use here in the absence of another explanation, is that dredge-up does not begin early enough on the TPAGB or at a low enough (core) mass in full stellar evolution models. This inability of stellar models to match the observed CSLFs in the Magellanic Clouds leads us to introduce two free parameters, $\Delta M_\mathrm{c}^\mathrm{min}$ and λ_min, which are used to calibrate our theoretical luminosity function. The minimum core mass for third dredge-up is shifted by $\Delta M_\mathrm{c}^\mathrm{min}(<0)$ such that dredge-up occurs at lower core masses than predicted by K02 (Fig. 9, left-hand panel). The dredge-up efficiency λ reaches the asymptotic value λ_max after a few pulses. We adjust it so that

$$\lambda_\mathrm{max} = \max\left(\lambda_\mathrm{min}, \lambda_\mathrm{max}^\mathrm{fit}\right), \tag{66}$$

where $\lambda_\mathrm{max}^\mathrm{fit}$ is the value from K02 (see Fig. 9, right-hand panel). The efficiency of dredge-up in low-mass stars is increased with to the fit of K02 but remains suppressed for the first few pulses (equation 48). Our synthetic model is used to calibrate values of $\Delta M_\mathrm{c}^\mathrm{min}$ and λ_min appropriate for the LMC ($Z = 0.008$) and SMC ($Z = 0.004$) by a least-squares minimization. The shifting of the dredge-up parameters in this way is motivated by simplicity in the face of ignorance of the physical process responsible for dredge-up in low-mass stars – a more complicated expression is not justified.

Our best-fitting single-star models have $\Delta M_\mathrm{c}^\mathrm{min} = -0.07$ and $\lambda_\mathrm{min} = 0.5$ for the LMC and $\Delta M_\mathrm{c}^\mathrm{min} = -0.07$ and $\lambda_\mathrm{min} = 0.65$ for the SMC with the VW93 wind with a superwind at a Mira period of 500 d. These values are similar to those of Marigo (2001), noting that $\Delta M_\mathrm{c}^\mathrm{min} = -0.07$ gives $M_\mathrm{c}^\mathrm{min} \approx 0.59\ \mathrm{M}_\odot$ at $M_\mathrm{i} \approx 1.5\ \mathrm{M}_\odot$ (a typical mass for C-stars: Wallerstein & Knapp 1998).

A simple linear fit to the above dredge-up parameters gives

$$\Delta M_\mathrm{c}^\mathrm{min} = -0.07 \tag{67}$$

and

$$\lambda_\mathrm{min} = 0.8 - 37.5Z \tag{68}$$

which equates to 0.05 at $Z = \mathrm{Z}_\odot$. Fig. 10 shows our resulting CSLFs.

Comparison with Fig. 5 shows that a value of $\Delta M_\mathrm{c}^\mathrm{min}$ nearer to $-0.09\ \mathrm{M}_\odot$ is necessary to match Marigo's prescription although the functional form of the prescription is otherwise similar.

5.3 Number ratios

We briefly consider the C/late-M number counts using the observations compiled by Groenewegen (2002) and the spectral type table of Jaschek & Jaschek (1995). We assume the CSLF dredge-up calibration above as our standard model and a constant star formation rate. It turns out to be very difficult to match the number ratios with our models unless we again change our free parameters. A good LMC fit ($\Delta M_\mathrm{c}^\mathrm{min} = -0.09$, $\lambda_\mathrm{min} = 0.7$, see Table 8) is obtained by increasing the amount of dredge-up, but then the CSLF peak is too dim. The SMC behaves in the opposite direction, with a decrease in the amount of dredge-up ($\Delta M_\mathrm{c}^\mathrm{min} = -0.06$, $\lambda_\mathrm{min} = 0.4$, see Table 9) which leads to a good fit but then the CSLF peak is too bright. We also show the effect of choosing a different wind prescription, with an $\eta = 3$ Reimers rate (Kudritzki & Reimers 1978) giving an even poorer fit than the VW93 wind (and too many bright stars in the CSLF). There are, however, many caveats to this simple approach. First, we have neglected the effect of a varying star formation

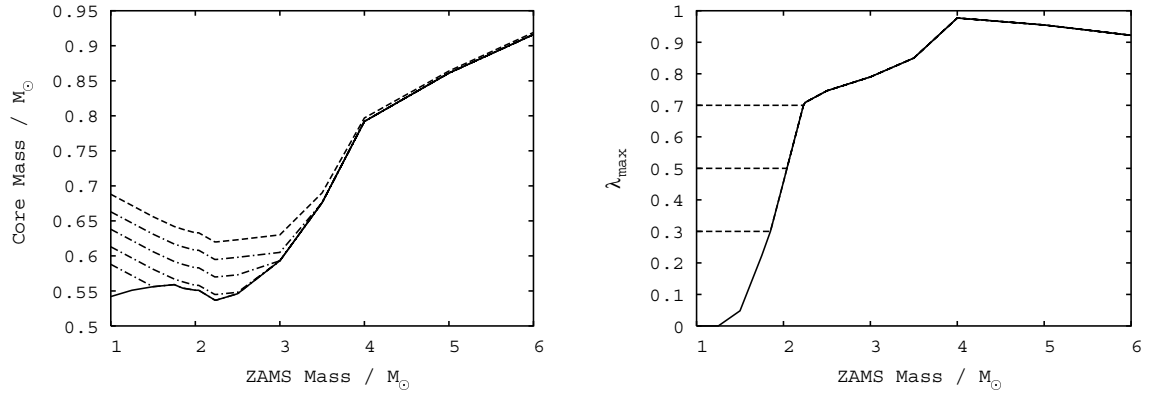

Figure 9. Left-hand panel: the solid line is the core mass at the first thermal pulse and the dashed line is $M_{\rm c}^{\rm min}$, both from Karakas et al. (2002) for $Z = 0.02$. The dot–dashed lines, from top to bottom, are for $\Delta M_{\rm c}^{\rm min} = 0$, -0.025, -0.05, -0.075 and -0.1. Right-hand panel: the solid line is $\lambda_{\rm max}$ from Karakas et al. (2002) for $Z = 0.02$; the dashed lines are, from bottom to top, for $\lambda_{\rm min} = 0.3$, 0.5 and 0.7.

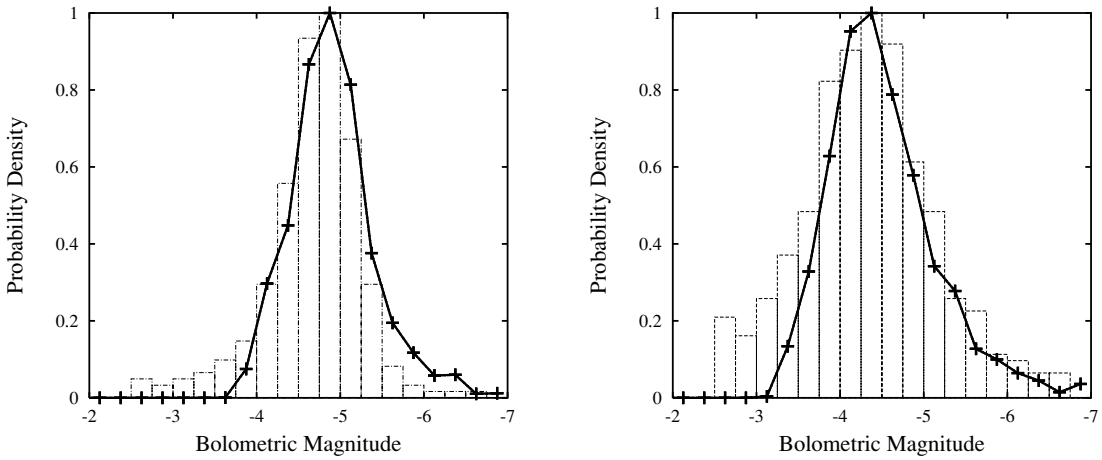

Figure 10. Our best-fitting carbon star luminosity functions for the LMC ($Z = 0.008$, left-hand panel) and the SMC ($Z = 0.004$, right-hand panel). Observations are from Groenewegen (2002).

rate which can be important when comparing number ratios (see Mouhcine & Lançon 2003). Secondly, the ratios are highly dependent on the spectral type which in turn depends on the stellar radius. It proved to be very difficult to fit the radius so any slight error on the fit leads to a resulting error in C/M. Thirdly, we neglect binary stars which produce giant branch and EAGB carbon stars (Izzard & Tout 2004). Fourthly, we do not take into account any observational selection effect, which is effectively the same as the assumption that the M-star surveys of the LMC and SMC are complete. This is unlikely to be true, while the C-star surveys (and resulting luminosity functions) are thought to be complete, although this helps us with the LMC and not the SMC. To simulate a magnitude-limited survey is beyond the scope of this paper. Since there is no systematic effect we will continue, in our ignorance, to use the dredge-up prescription calibrated by the CSLF.

5.4 Initial–final mass relation

The initial–final mass ($M_{\rm i}$–$M_{\rm f}$) relation is another check on the consistency of our models. Our synthetic results, including the dredge-up calibration, are plotted against the relation derived by Weidemann (2000) in Fig. 11. Weidemann 2000's results are partly based on evolution models and partly on observation, so it is difficult to draw any firm constraints from this comparison. The agreement is excellent for our $Z = 0.02$ models while the $Z = 0.004$ models are systematically high but always within 0.1 $\rm M_\odot$. The effect of the choice of mass-loss prescription at intermediate metallicity ($Z = 0.008$) is shown in Fig. 12, where we use the rates of Kudritzki &

Table 8. LMC number counts (see text for details).

LMC	Obs	Model	$\Delta M_{\rm c}^{\rm min} = -0.09$ $\lambda_{\rm min} = 0.7$	Model with Reimers $\eta = 3$
$\log_{10} N_{\rm C}/N_{\rm M3+}$	-0.0	-0.0	-0.0	-0.0
$\log_{10} N_{\rm C}/N_{\rm M5+}$	-0.0	-0.0	-0.0	-0.0
$\log_{10} N_{\rm C}/N_{\rm M6+}$	0.0	-0.0	0.0	-0.0

Table 9. SMC number counts (see text for details).

SMC	Obs	Model	$\Delta M_{\rm c}^{\rm min} = -0.06$ $\lambda_{\rm min} = 0.4$	Model with Reimers $\eta = 3$
$\log_{10} N_{\rm C}/N_{\rm M3+}$	-0.0	-0.0	-0.0	-0.0
$\log_{10} N_{\rm C}/N_{\rm M5+}$	0.0	0.0	0.0	0.0
$\log_{10} N_{\rm C}/N_{\rm M6+}$	1.19	1.65	1.36	0.0

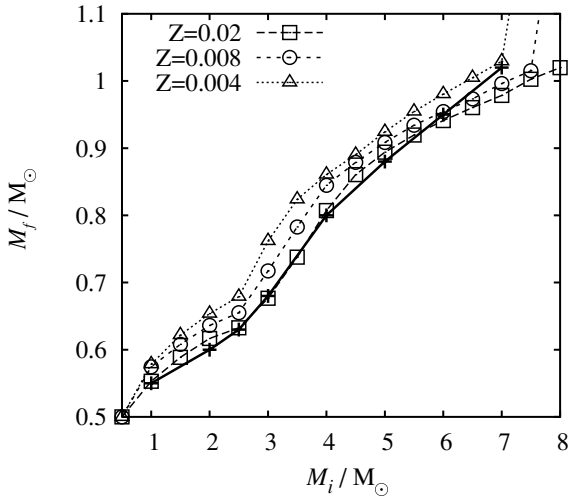

Figure 11. Final mass versus initial mass for stars with $0.5 \leqslant M_{\rm i}/{\rm M}_\odot \leqslant 8$ with metallicities 0.02 (squares), 0.008 (circles) and 0.004 (triangles) as calculated with the synthetic model (including dredge-up calibration). The solid line shows data from Weidemann (2000). Above $M_{\rm i} \approx 7$ M$_\odot$ the final mass is strongly metallicity-dependent because low-metallicity stars explode as supernovae on the EAGB, forming more massive neutron stars rather than white dwarfs.

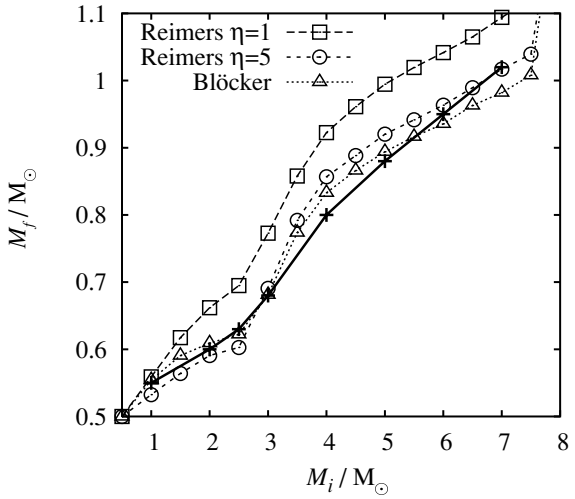

Figure 12. Final mass versus initial mass for $Z = 0.008$ with varying TPAGB mass-loss prescriptions: squares and circles are Reimers' rates with $\eta = 1$ and 5 respectively; triangles are Blöcker's rate with $\eta = 0.1$.

Reimers (1978) and Blöcker (1995). No single mass-loss relation gives the best agreement, but a Reimers $\eta = 1$ rate is discrepant by more than 0.1 M$_\odot$ for $M_{\rm i} \gtrsim 3$ M$_\odot$, perhaps ruling this out.

5.5 White dwarf mass distribution

The observed white dwarf mass distribution provides an additional constraint on our models. The inherent uncertainty in the initial–final mass relation, which is due to the use of evolutionary models to calculate an initial mass, is removed. The comparison of our synthetic white dwarf mass distribution with observations is shown in Fig. 13. The observations are compiled from Bergeron, Saffer & Liebert (1992), Bergeron, Liebert & Fulbright (1995), Bragaglia, Renzini & Bergeron (1995), Dreizler & Werner (1996), Bergeron, Ruiz & Leggett (1997), Finley, Koester & Basri (1997), Marsh et al. (1997), Vennes et al. (1997), Napiwotzki, Green & Saffer (1999), Vennes (1999), Bergeron, Leggett & Ruiz (2001), Claver et al. (2001) and Silvestri et al. (2001), with no attempt to take into account any observational selection effects such as dimming of old white dwarfs or systematic biases such as the effect of a binary companion, metallicity or errors inherent in different white dwarf mass determination techniques (although for duplicate stars the newer data are believed over the old). The data are plotted as a histogram in 10 bins, with an equal number of stars in each bin. Our synthetic model curves for $Z = 0.02$, 0.008 and 0.004 are calculated with 10^5stars for each metallicity between 0.1 and 8.0 M$_\odot$ and are binned in an identical way. Our dredge-up calibration of Section 5.1 is used. The initial mass function of KTG93 is used to calculate the contribution of each star to the histogram, and no attempt is made to mimic selection effects. The peak of the observations and theoretical curves are normalized to 1.0.

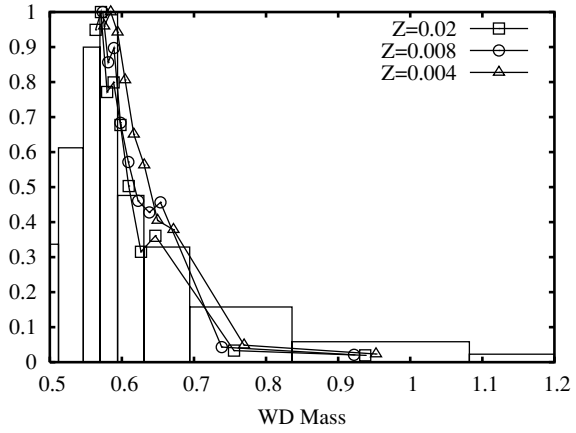

Figure 13. The white dwarf mass distribution. The boxed histogram shows the observations; the lines show our synthetic results for $Z = 0.02$ (squares), 0.008 (circles) and 0.004 (triangles).

The peak position of the mass distribution is matched well by our synthetic models. We have a dearth of white dwarfs above 0.7 M$_\odot$ and below about 0.55 M$_\odot$. These are probably due to the omission of binary stars from our analysis. Binary-induced mass loss leads to low-mass helium white dwarfs and mergers to high mass (possibly oxygen–neon) white dwarfs.

6 SINGLE STAR YIELDS

In this section we calculate stellar yields appropriate for use in galactic chemical evolution models. We compare these yields with our full stellar evolution model yields and previously published yields of van den Hoek & Groenewegen (1997) and Marigo (2001).

6.1 Calculation of yields

The yield of isotope j from a star can be represented simply as the mass expelled into the interstellar medium in time t:

$$\Delta M_j = \int_0^t \dot{M}_j \, {\rm d}t, \tag{69}$$

or as a function of the initial mass and abundance:

$$p(j, M_{\rm i}) = \frac{1}{M_{\rm i}} \int_0^t \dot{M} \Delta X_j \, {\rm d}t, \tag{70}$$

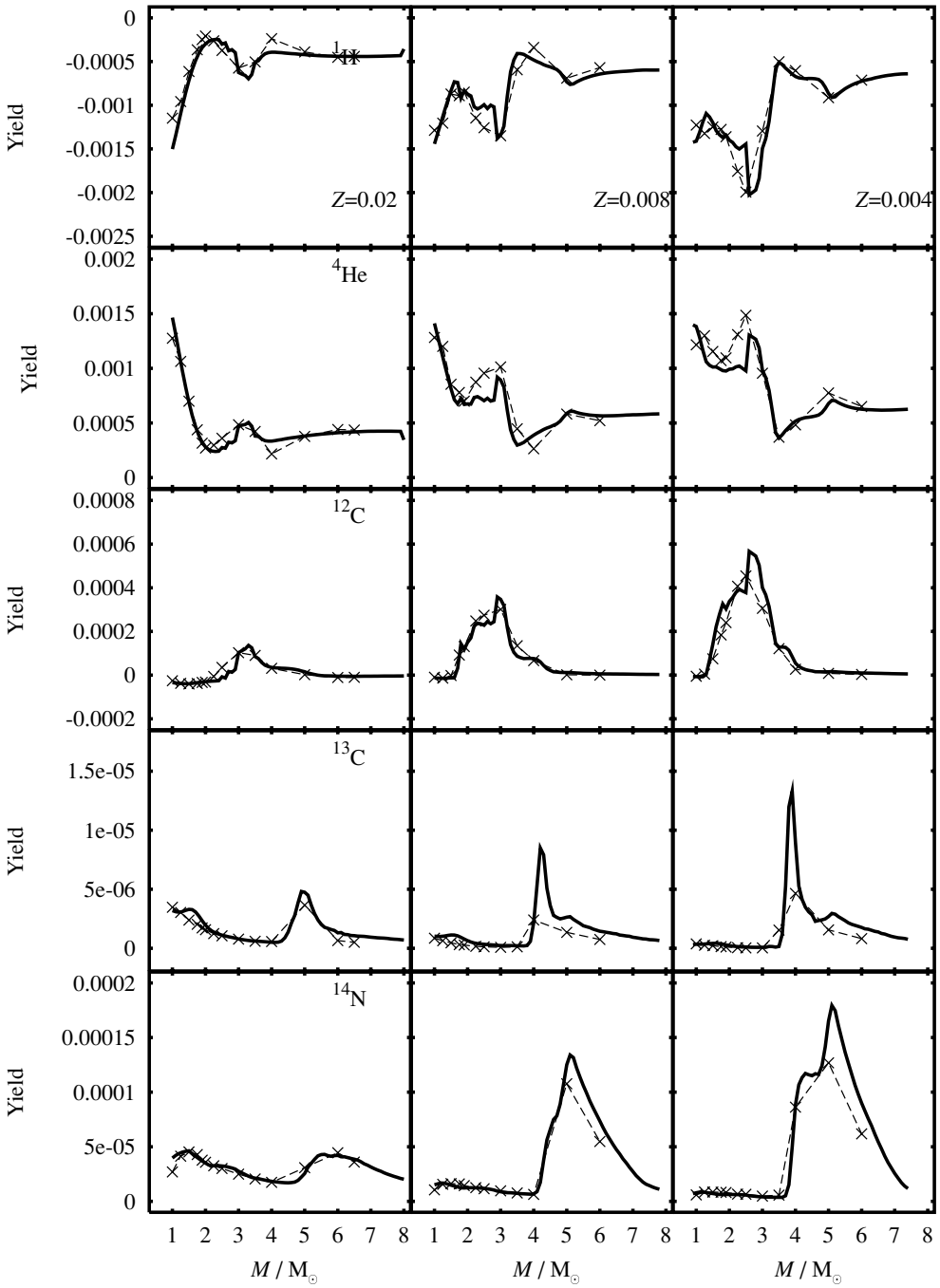

Figure 14. Synthetic HBB-calibrated, non-dredge-up-calibrated, initial mass function-weighted model yields y_j (solid lines) and our full stellar evolution model yields (dashed lines with crosses) versus initial mass for ^{1}H, ^{4}He, ^{12}C, ^{13}C and ^{14}N and $Z = 0.02$, 0.008 and 0.004.

where M_i is the initial mass of the star and $\Delta X_j = X_j(t) - X_j(0)$ is the change in surface abundance of species j between its birth and time t. The latter aids comparison with the models of van den Hoek & Groenewegen (1997) and Marigo (2001). Note that both these yields are independent of the initial mass function. A more useful definition of the yield is

$$y_j = \frac{\mathrm{d}Y_j}{\mathrm{d}M} = \xi(M_\mathrm{i}) \int_0^t \dot{M} \Delta X_j \, \mathrm{d}t = \xi(M_\mathrm{i}) M_\mathrm{i} p(j, M_\mathrm{i}), \qquad (71)$$

where $\xi(M_\mathrm{i})$ is the initial mass function [e.g. KTG93; $\xi(M_\mathrm{i})$ has units $\mathrm{M}_\odot^{-1}$ so y_j is dimensionless].

The integral

$$Y_j = \int_{M_1}^{M_2} y_j \, \mathrm{d}M \qquad (72)$$

is the total enrichment (in $\mathrm{M}_\odot$) of species j by a population of stars between masses M_1 and M_2.

The yield in equations (70) and (71) can be negative if an isotope is consumed (e.g. the hydrogen yield is always negative).

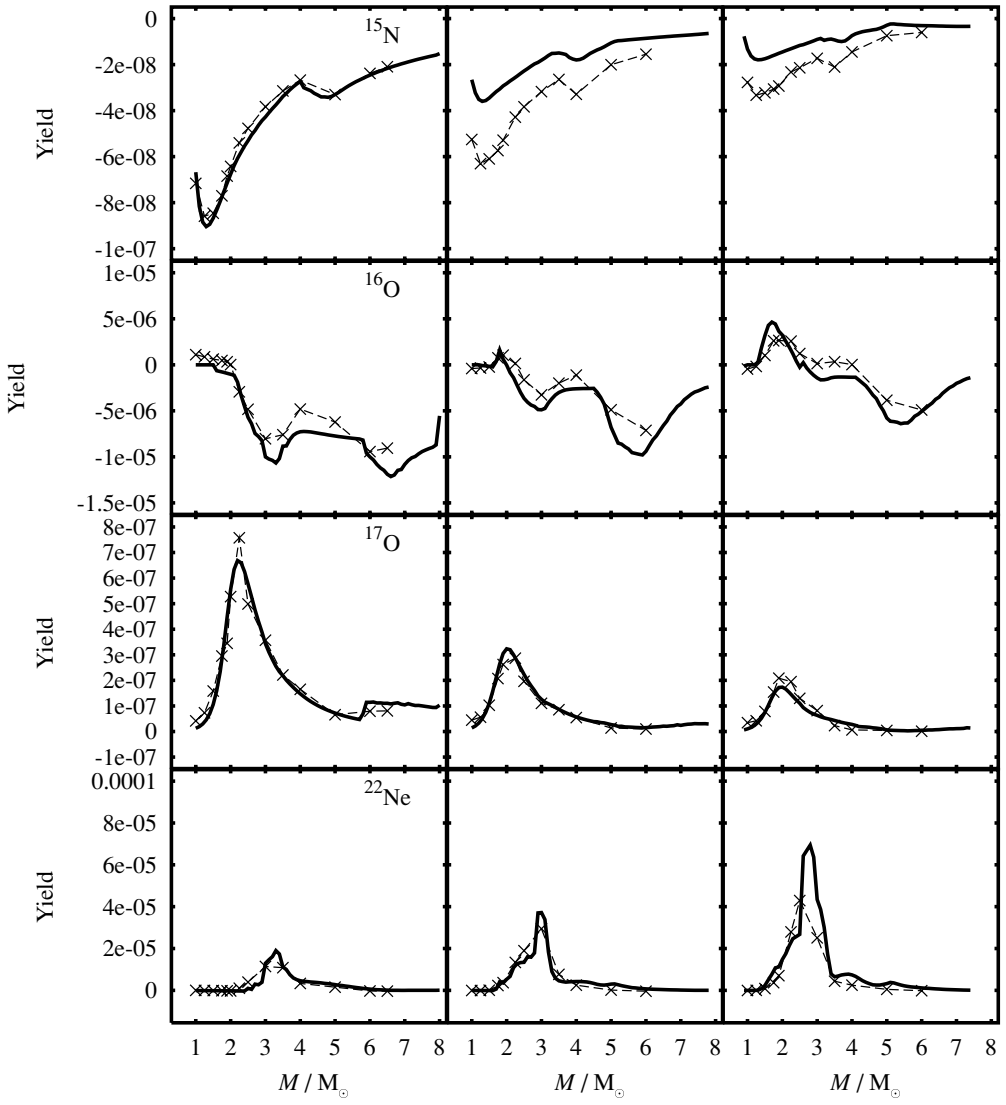

Figure 15. As Fig. 14, but for ^{15}N, ^{16}O, ^{17}O and ^{22}Ne.

The contributions to the yields are calculated from equation (71) at each time-step. The initial mass is in the range $0.1 \leqslant M_{\rm i}/{\rm M}_{\odot} \leqslant 8.0$. The stars are evolved for 16 Gyr and the yields (without supernova yields) shown are for the entire stellar lifetime. Full tables of yields are in Appendix D.[9] We show the yields from our full stellar evolution models without attempting to compensate for mass loss that would occur after model breakdown (see Karakas & Lattanzio 2003).

6.2 Results

Most of the mass from each star that is expelled in the stellar wind is hydrogen or helium, and most of this is expelled in the TPAGB stage of the evolution of the star. Stars with $M_{\rm i} \gtrsim 7$–8 M$_{\odot}$ do not have a TPAGB stage, but explode as supernovae first, so the stellar wind yield from these stars is negligible. Stars with $M_{\rm i} \lesssim 0.8$ M$_{\odot}$ do not evolve to the TPAGB in 16 Gyr so also have negligible yield. Comparison with the yields from (van den Hoek & Groenewegen 1997, (HG97), Marigo (2001) M01) and our full stellar evolution models is made. The yields of HG97 were calculated using a Kudritzki & Reimers (1978) mass-loss relation, with $\eta = 4$ (and $\eta = 2$ for $Z = 0.004$). The yields from M01 were calculated using the wind of VW93 (presumably with the $M_{\rm i} > 2.5$ M$_{\odot}$ correction) for $Z = 0.019$ (but we compare them with our $Z = 0.02$ models) and mixing length parameter $\alpha_{\rm MLT} = 1.68$ rather than 1.75.

6.2.1 Comparison with our full stellar evolution models

Figs 14 and 15 compare our synthetic model yields (equation 71) with our full stellar evolution model yields using the HBB calibration of Section 4, without the dredge-up calibration of Section 5.1 and with the KTG93 initial mass function weighting. Our synthetic model does an excellent job of reproducing our full stellar evolution models for all isotopes considered except ^{22}Ne. Slight overproduction of ^{12}C, ^{13}C and ^{14}N for $M_{\rm i} \gtrsim 5$ M$_{\odot}$ is due to small differences between our synthetic and full evolution models. The spike in production of ^{13}C at around $M_{\rm i} \approx 4$–5 M$_{\odot}$ is not an anomaly – rather it

[9] http://www.blackwellpublishing.com/products/journals/suppmat/mnr/mnr7446/mnr7446sm.htm

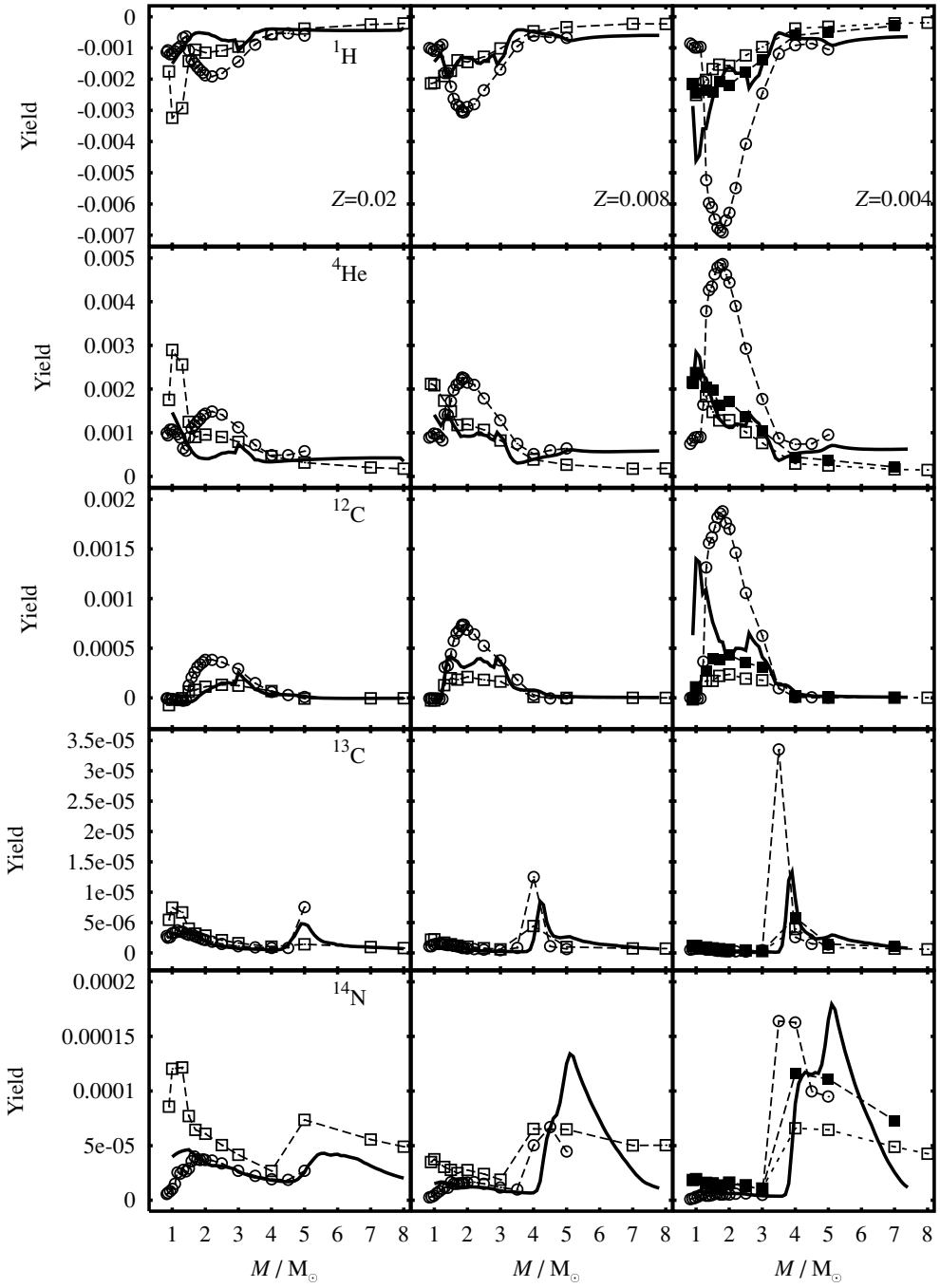

Figure 16. Our synthetic HBB- and dredge-up-calibrated model yields y_j (solid lines) versus other models (circles from M01, squares from HG97, filled symbols for $\eta = 2$, open symbols for $\eta = 4$) for ^{1}H, ^{4}He, ^{12}C, ^{13}C and ^{14}N and $Z = 0.02$, 0.008 and 0.004. An initial mass function weighting is included.

is not resolved on our full stellar evolution model mass grid unless it happens to lie on an integer multiple of $M_\odot$ (as is the case for $Z = 0.02$). We do not include ^{22}Ne destruction reactions so our synthetic yields are overestimates for $M_i \gtrsim 4\ M_\odot$.

6.2.2 *Comparison with other models*

We use the HBB and dredge-up calibrations made above (Sections 4 and 5.1) to compare our synthetic model yields with those of M01 and HG97. The yields are weighted with the KTG93 initial mass function – see Figs 16 and 17 and Appendix A7.

For most isotopes our yields lie between the values given by M01 and HG97. Our synthetic models experience less dredge-up than M01's in the range $1 \lesssim M_i/M_\odot \lesssim 3$, leading to a relative underproduction of carbon and oxygen, though slightly more than HG97. The ^{13}C spike position differs between our synthetic models and M01's by 0.5 $M_\odot$ at $Z = 0.004$, suggesting that we invoke HBB at a slightly higher mass, and also by a factor of about 2.5 (perhaps due to excess ^{12}C seed). At lower metallicities ($Z \leqslant 0.008$) we overproduce nitrogen compared with the other yield sets, but M01 does not have AGB stars above 5 $M_\odot$ and our results are not dissimilar to HG97's $Z = 0.004$, $\eta = 2$ case (they publish no

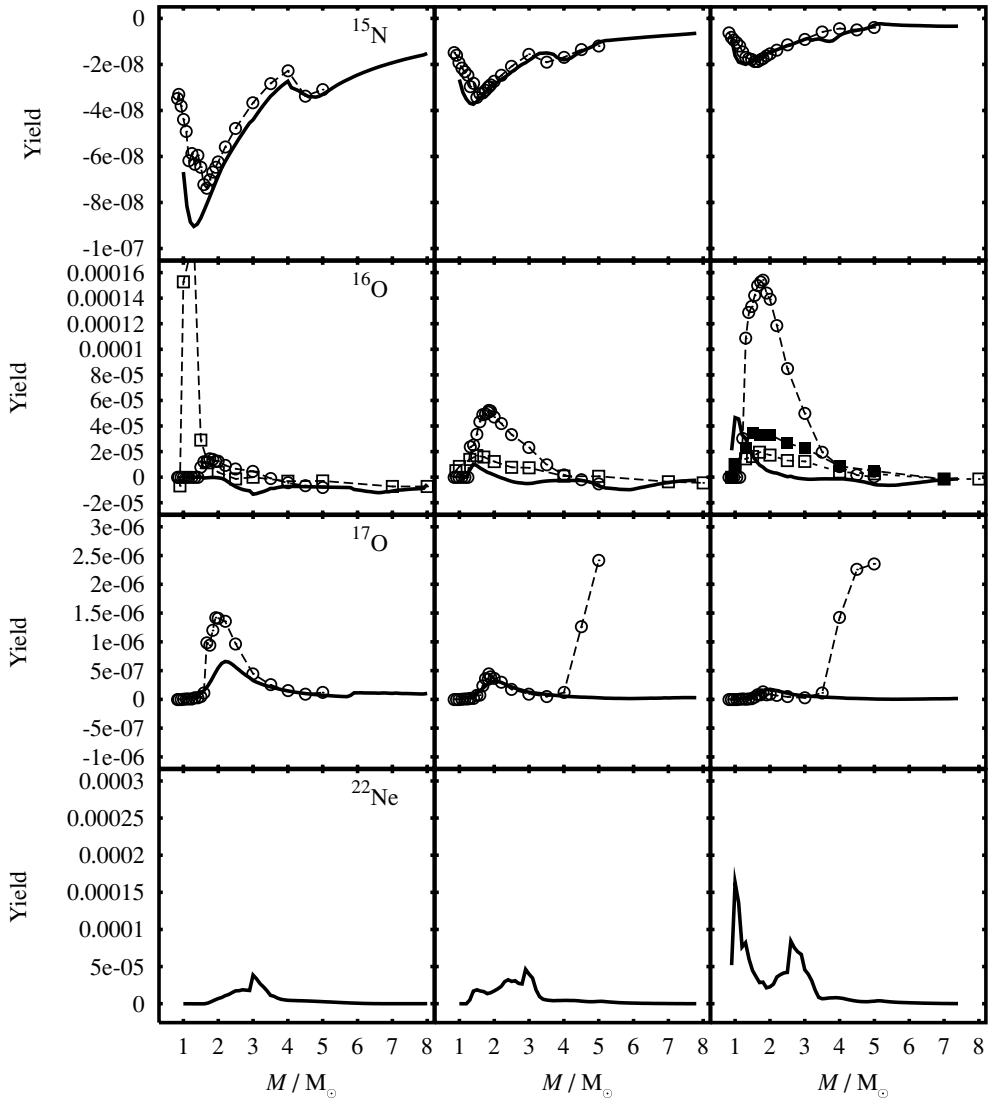

Figure 17. As Fig. 16 but for ^{15}N, ^{16}O, ^{17}O and ^{22}Ne.

$\eta = 2$ yields for $Z = 0.008$). Our ^{15}N agrees well with M01. The huge ^{16}O production at low mass in HG97's data set for $Z = 0.02$ cannot be reproduced, although otherwise our yields agree well except for the lack of oxygen from dredge-up compared with M01 (also our intershell abundance is on average about 1 per cent compared with Marigo's 2 per cent). We produce negligible ^{17}O compared with M01 although the amount is still rather small. The initial mass function-weighted ^{22}Ne yields show that the region of HBB ($M_{\rm i} \gtrsim 4$–5 M$_\odot$) is a relatively unimportant contributor to the total yield. It is also possible that the lower initial core masses from the Padova models have an effect on the evolution of M01's models, with lower core mass leading to lower luminosity and so a longer TPAGB phase with more dredge-up and enhanced CO yields.

7 CONCLUSIONS

We have presented a fast yet accurate synthetic model for TPAGB evolution based on state-of-the-art full evolution models. Yields calculated by the synthetic model and the full evolution model agree closely, with continuation of the synthetic model beyond the breakdown point of the detailed model for high-mass AGB stars. Calibration of third dredge-up to the Magellanic Cloud carbon star luminosity functions forces us to reduce our theoretically derived minimum mass for core mass by -0.07 M$_\odot$ and enforce a value of at least $0.8 - 37.5Z$ on the maximum dredge-up efficiency $\lambda_{\rm max}$. The calibrated yields in general lie between the previously published yields of van den Hoek & Groenewegen (1997) and Marigo (2001), although our models produce more nitrogen and less carbon at low metallicity. Our synthetic model fits the initial–final mass relation to within 0.1 M$_\odot$ and reasonably fits the observed white dwarf mass distribution (we require binary stars to fit it properly). The next step is to include this synthetic model in the Hurley et al. (2002) binary code, and much progress has already been made in this direction (Izzard & Tout 2004,2003).

ACKNOWLEDGMENTS

We thank John Lattanzio, Maria Lugaro, Richard Stancliffe, Carolina Ödman and especially the anonymous referee for useful discussion, encouragement and suggestions. RGI thanks PPARC for

a scholarship, Monash Mathematics Department for putting up with him, and his own pocket for decent computing facilities. CAT thanks Churchill College for a fellowship.

REFERENCES

Anders E., Grevesse N., 1989, Geochim. Cosmochim. Acta, 53, 197
Angulo C. et al., 1999, Nucl. Phys. A, 656, 3
Bergeron P., Saffer R. A., Liebert J., 1992, ApJ, 394, 228
Bergeron P., Liebert J., Fulbright M. S., 1995, ApJ, 444, 810
Bergeron P., Ruiz M. T., Leggett S. K., 1997, ApJS, 108, 339
Bergeron P., Leggett S. K., Ruiz M. T., 2001, ApJS, 133, 413
Blöcker T., 1995, A&A, 297, 727
Blöcker T., Schönberner D., 1991, A&A, 244, L43
Boothroyd A. I., Sackmann I.-J., 1988, ApJ, 328, 632
Bragaglia A., Renzini A., Bergeron P., 1995, ApJ, 443, 735
Busso M., Gallino R., Lambert D. L., Travaglio C., Smith V. V., 2001, ApJ, 557, 802
Chieffi A., Domínguez I., Limongi M., Straniero O., 2001, ApJ, 554, 1159
Claver C. F., Liebert J., Bergeron P., Koester D., 2001, ApJ, 563, 987
Clayton D. D., 1983, Principles of Stellar Evolution and Nucleosynthesis. Univ. Chicago Press, Chicago
Dray L. M., Tout C. A., Karakas A. I., Lattanzio J. C., 2003, MNRAS, 338, 973
Dreizler S., Werner K., 1996, A&A, 314, 217
Finley D. S., Koester D., Basri G., 1997, ApJ, 488, 375
Forestini M., Charbonnel C., 1997, A&AS, 123, 241
Frost C. A., 1997, PhD thesis, Monash University
Frost C. A., Lattanzio J. C., Wood P. R., 1998, ApJ, 500, 355
Girardi L., Bressan A., Bertelli G., Chiosi C., 2000, A&AS, 141, 371 (G00)
Groenewegen M. A. T., 1999, in Le Bertre T., Lebre A., Waelkens C., eds, Proc. IAU Symp. 191, Asymptotic Giant Branch Stars. Astron. Soc. Pac., San Francisco, p. 535
Groenewegen M. A. T., 2002, preprint (astro-ph/0208449)
Groenewegen M. A. T., de Jong T., 1993, A&A, 267, 410 (GdJ93)
Henry R. B. C., 2004, in McWilliam A., Rauch M., eds, Origin and Evolution of the Elements. Cambridge Univ. Press
Herwig F., 2000, A&A, 360, 952
Hurley J., 2000, PhD thesis, Univ. Cambridge
Hurley J. R., Pols O. R., Tout C. A., 2000, MNRAS, 315, 543
Hurley J. R., Tout C. A., Pols O. R., 2002, MNRAS, 329, 897 (H02)
Iben I., Renzini A., 1983, ARA&A, 21, 271
Iben I., Truran J. W., 1978, ApJ, 220, 980
Iglesias C. A., Rogers F. J., 1996, ApJ, 464, 943
Izzard R. G., Tout C. A., 2003, Publ. Astron. Soc. Aust., 20, 345
Izzard R. G., Tout C. A., 2004, MNRAS, in press
Jaschek C., Jaschek M., 1995, The Behavior of Chemical Elements in Stars. Cambridge Univ. Press
Karakas A. I., Lattanzio J. C., 2003, Publ. Astron. Soc. Aust., 20, 279
Karakas A. I., Lattanzio J. C., Pols O. R., 2002, Publ. Astron. Soc. Aust., 19, 515 (K02)
Kroupa P., Tout C., Gilmore G., 1993, MNRAS, 262, 545 (KTG93)
Kudritzki R., Reimers D., 1978, A&A, 70, 227
Lattanzio J. C., 1989, ApJ, 344, L25
Lattanzio J. C., Frost C. A., Cannon R. C., Wood P. R., 1997, in Advances in Stellar Evolution. Cambridge Univ. Press, p. 130
Marigo P., 1999, in Le Bertre T., Lebre A., Waelkens C., eds, Proc. IAU Symp. 191, Asymptotic Giant Branch Stars. Astron. Soc. Pac., San Francisco, p. 53 (M99)
Marigo P., 2001, A&A, 370, 194 (M01)
Marigo P., Bressan A., Chiosi C., 1998, A&A, 331, 564
Marigo P., Girardi L., Bressan A., 1999a, A&A, 344, 123
Marigo P., Girardi L., Weiss A., Groenewegen M. A. T., 1999b, A&A, 351, 161
Marsh M. C. et al., 1997, MNRAS, 286, 369
Mouhcine M., Lançon A., 2003,, MNRAS, 338, 572
Mowlavi N., 1999, A&A, 350, 73
Mowlavi N., Meynet G., 2000, A&A, 361, 959
Mowlavi N., Jorissen A., Arnould M., 1998, A&A, 334, 153
Napiwotzki R., Green P. J., Saffer R. A., 1999, ApJ, 517, 399
Paczynski B., 1970, Acta Astron., 20, 47
Press W. H., Teukolsky S. A., Vetterling W. T., Flannery B. P., 1992, Numerical Recipes in C. The Art of Scientific Computing, 2nd edn. Cambridge Univ. Press, Cambridge
Renzini A., Voli M., 1981, A&A, 94, 175
Russell S. C., Dopita M. A., 1992, ApJ, 384, 508
Silvestri N. M., Oswalt T. D., Wood M. A., Smith J. A., Reid I. N., Sion E. M., 2001, AJ, 121, 503
Straniero O., Chieffi A., Limongi M., Busso M., Gallino R., Arlandini C., 1997, ApJ, 478, 332
Tuli J., 2000, Nuclear Wallet Cards. Brookhaven National Laboratory
van den Hoek L. B., Groenewegen M. A. T., 1997, A&AS, 123, 305 (HG97)
Vassiliadis E., Wood P. R., 1993, ApJ, 413, 641 (VW93)
Vennes S., 1999, ApJ, 525, 995
Vennes S., Thejll P. A., Galvan R. G., Dupuis J., 1997, ApJ, 480, 714
Wagenhuber J., Groenewegen M. A. T., 1998, A&A, 340, 183
Wallerstein G., Knapp G. R., 1998, ARA&A, 36, 369
Weidemann V., 2000, A&A, 363, 647
Wood P. R., Zarro D. M., 1981, ApJ, 247, 247

This paper has been typeset from a TEX/LATEX file prepared by the author.